Articles

A Structure-Based Approach to a Synthetic Vaccine for HIV-1[†]

Edelmira Cabezas,[‡] Meng Wang,[§] Paul W. H. I. Parren,[§] Robyn L. Stanfield,[||] and Arnold C. Satterthwait*[,‡]

The Burnham Institute, 10901 Torrey Pines Road, La Jolla, California 92037, and Departments of Immunology and Molecular Biology, The Scripps Research Institute, 10550 North Torrey Pines Road, La Jolla, California 92037

Received February 16, 2000; Revised Manuscript Received August 14, 2000

ABSTRACT: The generation of neutralizing antibodies by peptide immunization is dependent on achieving conformational compatibility between antibodies and native protein. Consequently, approaches are needed for developing conformational mimics of protein neutralization sites. We replace putative main-chain hydrogen bonds (NH → O═CRNH) with a hydrazone link (N−N═CH−CH_2CH_2) and scan constrained peptides for fit with neutralizing monoclonal antibodies (MAbs). To explore this approach, a V3 MAb 58.2 that potently neutralizes T-cell lab-adapted HIV-1_{MN} was used to identify a cyclic peptide, [JHIGPGR-(Aib)F(D-Ala)GZ]G-NH_2 (loop 5), that binds with >1000-fold higher affinity than the unconstrained peptide. NMR structural studies suggested that loop 5 stabilized β-turns at GPGR and R(Aib)F(D-Ala) in aqueous solvent implying considerable conformational mimicry of a Fab 58.2 bound V3 peptide determined by X-ray crystallography [Stanfield, R. L. et al. (1999) *Structure 142*, 131−142]. Rabbit polyclonal antibodies (PAbs) generated to loop 5 but not to the corresponding uncyclized peptide bound the HIV-1_{MN} envelope glycoprotein, gp120. When individual rabbit antisera were scanned with linear and cyclic peptides, further animal-to-animal differences in antibody populations were characterized. Loop 5 PAbs that most closely mimicked MAb 58.2 neutralized HIV-1_{MN} with similar potency. These results demonstrate the remarkable effect that conformation can have on peptide affinity and immunogenicity and identify an approach that can be used to achieve these results. The implications for synthetic vaccine and HIV-1 vaccine research are discussed.

The development of broadly cross-reactive neutralizing antibodies is an important aim of HIV-1[1] vaccine research (*1*, *2*). However, the HIV-1 envelope glycoproteins, gp120 and gp41, are poorly immunogenic (*1*, *2*). HIV-1 has also undergone an unprecedented degree of mutation (*3*) that complicates vaccine design. Sera from HIV-1 seropositive individuals generally neutralize HIV-1 very poorly. Nevertheless, antisera from a subset of long-term nonprogressors show a marked broadening of HIV-1 neutralizing activities, and a few potent neutralizing monoclonal antibodies have been identified (*2*, *4*, *5*). There is a critical need for approaches to identify and recapitulate these activities.

Antibodies are often identified and their specificities characterized with peptides (*6*). Peptides can in turn be used to generate antibodies which in some cases are neutralizing (*7*). While the availability of peptides favor the approach, it is limited by conformational issues (*8*−*10*). Peptides are conformationally heterogeneous in aqueous solution (*11*), often differing from the structures their cognate sequences adapt in native proteins. This has two important consequences. First, it reduces the affinity of peptides for antibodies generated by native proteins (*8*, *9*, *12*). For a peptide to bind a native protein antibody, it must approximate the native conformation with a cost in free energy that can significantly lower affinity (*12*). Second, the binding pockets of antipeptide antibodies reflect the conformational heterogeneity of peptides (*13*) and are for the most part incompatible with native protein surfaces (*10*, *11*, *13*−*15*).

[†] This work was supported by the National Institutes of Health (AI37512 to A.C.S. and GM46192 to I.A.W. for R.L.S.) and The Department of Defense, Army (DAMD17-95-2-5017 to A.C.S.).

* To whom correspondence should be addressed: Phone: 858-646-3100, ext. 3658. Fax: 858-646-3195. E-mail: asat@burnham-inst.org.

[‡] The Burnham Institute.

[§] Department of Immunology, The Scripps Research Institute.

[||] Department of Molecular Biology, The Scripps Research Institute.

[1] Abbreviations: TCLA, T-cell lab-adapted; HIV-1, human immunodeficiency virus type 1; MN, HIV-1_{MN}; IIIB, HIV-1_{IIIB}; JR-CSF, HIV-1_{JRCSF}; rgp120, baculovirus-derived recombinant envelope glycoprotein 120_{MN}; p24, HIV-1 protein; MAb, monoclonal antibody; Fab, antigen binding fragment; PAbs, polyclonal antibodies; Aib, α,α-dimethylglycine; NMP, *N*-methylpyrrolidone; DIC, 1,3-diisopropylcarbodiimide; HOBt, 1-hydroxybenzotriazole; DIEA, diisopropylethylamine; DCM, dichloromethane; AN, acetonitrile; TFE, trifluroethanol; MS, mass spectrometry; MAPS, multiple-antigen-peptide system; ELISA, enzyme-linked immunosorbent assay; PBS, phosphate-buffered saline; pNPP, *p*-nitrophenyl phosphate; EC_{50}, effective concentration of peptide that inhibited 50% of the binding of antibody to plate-bound antigen; IC_{90}, concentration (or titer) of antibody that inhibited ≥90% of HIV-1 infectivity; $TCID_{50}$, 50% tissue culture infective dose; NOESY, nuclear Overhauser effect spectroscopy; ROESY, rotating-frame Overhauser effect spectroscopy; TOCSY, total correlation spectroscopy; P. E. COSY, phase-edited correlation spectroscopy; TPPI, time-proportional phase incrementation.

10.1021/bi0003691 CCC: $19.00
Published on Web 11/01/2000

Table 1: Linear, Cyclic Peptides and MAPS Prepared for This Study[a]

peptide	sequence
MN	**I1−H2−I3−G4−P5−G6−R7−A8−F9−Y10**
linear 1	Ac-GHIGPGRAFGGG-NH_2
linear 2	Ac-GHIGPGRAFGGGG-NH_2
linear 3	Ac-GHIGP(D-Ala)RAFGGGG-NH_2
linear 4	Ac-GHIGPGR(Aib)FGGGG-NH_2
linear 5	**AcG1−H2−I3−G4−P5−G6−R7−(Aib)8−F9−(D-Ala)10−GGG-NH_2**
linear 5/C	Ac-GHIGPGR(Aib)F(D-Ala)GGC-NH_2
loop 1	[JHIGPGRAFGZ]G-NH_2
loop 2	[JHIGPGRAFGGZ]G-NH_2
loop 3	[JHIGP(D-Ala)RAFGGZ]G-NH_2
loop 4	[JHIGPGR(Aib)FGGZ]G-NH_2
loop 5	**[J−H2−I3-G4-P5-G6-R7-(Aib)8-F9-(D-Ala)10-GZ]G-NH_2**
loop 5/C	[JHIGPGR(Aib)F(D-Ala)GZ]C−NH_2
loop 6	Ac-[CHIGPGR(Aib)FGGC]-NH_2
loop 7	[JHVGPGR(Aib)F(D-Ala)GZ]G-NH_2
MAPS core	(chloro-Ac{TT2}$KKK)_4(KGG)_2$KA-NH_2
linear 5-MAPS	(linear 5/C−Ac-{TT2}$KKK)_4(KGG)_2$KA-NH_2
loop 5-MAPS	(loop 5/C−Ac-{TT2}$KKK)_4(KGG)_2$KA-NH_2

[a] The MN sequence was renumbered; **I1** (our numbering) is I312 from the MN sequence (*3*). The same numbering system was used for the peptides as shown for linear 5 and loop 5. The single letter code is used for standard amino acids. D-Ala is D-alanine; Aib is α,α-dimethylglycine; J and Z are linking residues used to form the hydrazone link which is indicated by brackets; Ac is acetyl; chloro-Ac is chloroacetyl; -NH_2 represents a C-terminal carboxamide and {TT2} is a tetanus toxoid T-helper epitope, QYIKANSKFIGITEL. MAPS structures are depicted in Figure 7 and Supporting Information.

The immunological activities of peptides can, however, be improved by constraining them to mimic protein substructures (*8*, *16*−*18*). This expedient though needs synthetic methods that can be used to broaden the approach (*17*). Recently, two of us reported a solid-phase synthetic method for replacing main-chain hydrogen bonds (NH → O═CRNH) with a hydrazone covalent mimic (NN═CH−CH_2CH_2) (*19*). On average, about 60% of the amino acids in globular proteins engage in main-chain hydrogen bonds (*20*). Since protein substructures can be distinguished by differences in hydrogen bonding patterns (*19*), we reasoned that the hydrazone link might be used to constrain peptides to different conformations depending on where it was positioned in the peptide (*19*). Indeed, the hydrazone link has been used to constrain short peptides as α-helices (*19*) and loops (*21*). It is also chemically stable in aqueous solution at physiological temperature and pH as required of immunogenic peptides (*19*).

Since the hydrazone link satisfied important criteria, we decided to test whether it could improve the antigenicity (affinity for antibodies) and immunogenicity (generation of neutralizing antibodies) of a short peptide from the V3 loop. The V3 loop is a 35-residue (± 2 residues) disulfide loop on gp120 that encompasses a neutralizing epitope on TCLA HIV-1 viruses (*22*). V3 peptides have provided important testing grounds for synthetic vaccine approaches (*23*−*27*). Interest in the V3 loop has also led to the identification of potent neutralizing V3 MAbs (*28*−*30*). We decided to use one of these MAbs to explore the antigenicity of hydrazone-linked peptides with the goal of identifying a constrained peptide mimetic of the MAb bound conformer using enhanced affinity as a measure of fit. The mimetic could then in turn be tested as an immunogen.

We relied mostly on MAb 58.2 (*30*) as a template for our studies. MAb 58.2 potently neutralizes TCLA HIV-1_{MN} and binds a V3 epitope that encompasses a short neutralizing determinant (SND), IGPGRAF, that is shared by the majority of Clade B HIV-1 viruses (*22*). X-ray crystallography of Fab 58.2-peptide complexes were being pursued and became available during the course of this project (*21*). Essentially, we found that constraining a short V3 peptide with the hydrazone link enhanced its affinity for MAb 58.2. This identified a cyclic peptide that showed considerable mimicry of the MAb 58.2 bound conformer by NMR spectroscopy. In turn, we found that the mimetic was a far better immunogen than the corresponding unconstrained peptide demonstrating the effectiveness of this approach.

MATERIALS AND METHODS

Peptide Synthesis. Linear and cyclic peptides were synthesized by solid-phase methods. Side chains were protected using Fmoc-His(Trt), Fmoc-Arg(Pbf), Fmoc-Cys(Trt), Fmoc-Lys(Boc), and Fmoc-Lys(Fmoc). Peptides were purified with Gilson analytical and preparative HPLC systems using linear gradients formed from solvent systems A: 0.1% TFA/H_2O (v/v) and B: 0.1% TFA/AN (v/v).

Linear peptides (Table 1) were synthesized with an ACT-350 multiple peptide synthesizer (Advanced Chem Tech) on Rink amide resin (0.4−0.6 mmol/g) using standard Fmoc synthesis with DIC/HOBt coupling. The N-termini of peptides were acetylated on the resin with 15% acetic anhydride in DMF. The acetylated peptides were cleaved with Reagent K (*31*), precipitated with diethyl ether and purified using a preparative RP C-18 column (Cosmosil 5C18-AR, 2 × 25 cm) eluting at 8 mL/min with a 0−50% AN gradient over 30 min. Peptides were confirmed by FAB MS or ES MS.

Cyclic hydrazone-linked peptides (Table 1) were synthesized by solid-phase synthesis on Rink amide resin (0.4−0.6 mmol/g) according to Scheme 1 using previously described procedures (*19*). These syntheses required the prior preparation of J and Fmoc-Z(Act) (*19*). *N*-α-Fmoc-glycine chloride was prepared according to Carpino et al. (*32*) and shown to be >98% acyl chloride by the methanol test (*32*). Initially, Fmoc-GZ(Act)G/C(Trt)-resin was synthesized manually in resin packets (*19*). The most critical step was the coupling of Fmoc-Gly chloride to Z(Act). Fmoc-Gly chloride was freed of trace HCl under vacuum before use, mixed with

Scheme 1

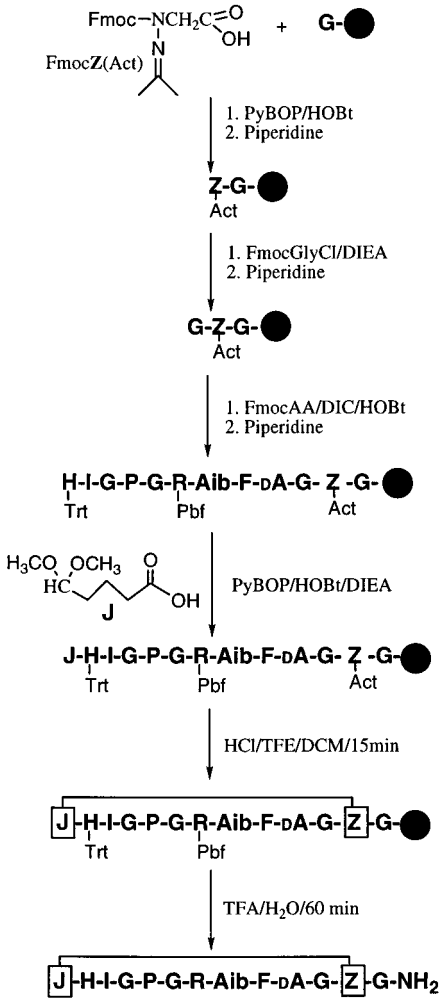

NMP, and briefly shaken with Z(Act)G/C(Trt)-Resin before adding DIEA (*19*). The product, Fmoc-GZ(Act)G/C(Trt)-resin, was removed from the resin packet and transferred to the ACT-350 peptide synthesizer where it was extended using standard Fmoc synthesis. The addition of Fmoc-Arg(Pbf) to Aib was the only difficult coupling step, proceeding ≈60% despite triple coupling. After adding the final amino acid, Fmoc-His(Trt), the peptide-resin was transferred to resin packets, the Fmoc group removed with piperidine, the peptide capped with J and then rapidly cyclized in acidic 20% TFE/DCM *(19)*. Cyclic peptides were cleaved from the resin and deprotected with 5% H_2O/95% TFA and precipitated with diethyl ether. Thiol scavengers were excluded from the cleavage reaction since high concentrations of free thiol in TFA destroy the hydrazone link (*19*). The cyclic peptides were typically purified by HPLC using a preparative RP C-18 column (Cosmosil, 5C18-AR) eluting at 8 mL/min with a 0−20% AN gradient over 5 min followed by 20−40% AN over 30 min (Supporting Information). The yields of cyclic hydrazone-linked peptides (based on resin loading) were ≈5−10%. Each purified cyclic peptide showed one peak by HPLC and was confirmed by FAB MS or ES MS.

The disulfide loop 6 (Table 1) was initially prepared as a linear peptide using Fmoc-Cys(Trt) and cleaved from the resin with Reagent K as described above. The linear peptide (1 mg/mL) was quantitatively cyclized in 20% DMSO/H_2O, pH 4.0, in 1 day (*33*). After confirming the loss of free thiol using Ellman's test (*34*), the reaction mixture was lyophilized and loop 6 was purified by HPLC on a RP-C18 column and confirmed by ES MS.

MAPS Synthesis. MAPS (*35*) were modified (*36, 37*) and prepared for immunizations using a chemical ligation protocol (*37*). First, a chloroacetylated MAPS core (Table 1) was synthesized on TGR resin (NovaBiochem, 0.1 mmol/g) with the ACT-350 synthesizer using Fmoc synthesis. *N*-α-Fmoc-Lys(Fmoc) was used at the branch points. The N-termini of the four branches of the MAPS core were chloroacetylated on the resin with 10 equiv of chloroacetic acid anhydride in DMF for 15 min. The chloroacetylated MAPS core was cleaved from the resin and deprotected by treating it with 5% H_2O/95% TFA for 1 h. It was then precipitated with cold diethyl ether, lyophilized, and purified by HPLC on a preparative RP C4 column (Vydac, 214TP1022, 2.2 × 25 cm) eluting at 15 mL/min with a 0−20% AN gradient over 10 min followed by a 20−30% AN over 20 min. Pure chloroacetylated MAPS core (5% yield) was identified by ES MS: calcd (MH+), 9377, obs 9374 (Supporting Information).

Second, linear 5/C or loop 5/C (Table 1) were chemically ligated to the chloroacetylated MAPS core. A 5-fold molar excess (relative to chloroacetylated arms) of linear 5/C (2.8 mg) or loop 5/C (2.7 mg) was mixed with chloroacetylated MAPS core (1.0 mg) in 0.5 mL degassed 0.5 M Tris, pH 8.9, and 3 M guanidinium·HCl containing 8 mM EDTA under nitrogen. The reactions were monitored on an analytical RP C4 column (Vydac, 214TP54) eluting at 2 mL/min with a 0−20% AN gradient over 10 min followed by a 20−32% AN over 30 min (Supporting Information). The reaction appeared complete after 2 h but was continued overnight to ensure a complete reaction. The products were purified on the preparative RP C4 column (Vydac, 214TP1022) eluting at 15 mL/min with a 0−20% AN gradient for 5 min followed by a 20−35% AN for 30 min. These purifications yielded 0.8 mg of linear 5-MAPS (52% yield based on MAPS core) and 0.6 mg of loop 5-MAPS (40% yield) which were stored dry at − 20 °C. Both MAPS were soluble in water. Linear 5-MAPS was identified by ES MS: calcd (MH+), 14244, obs 14245. Loop 5-MAPS was identified by MALDI MS: calcd (MH+), 14228, obs 14223 (Supporting Information).

Immunization. Linear 5-MAPS and loop 5-MAPS were prepared in separate lots for immunizations by dissolving them in deionized water and vigorously mixing with an equal volume of twice the recommended concentration of RIBI adjuvant system R-730 (RIBI ImmunoChem Research, Inc) in PBS. Each rabbit (NZW female, 2−2.5 kg) was immunized with 1 mL of emulsion at multiple sites (subcutaneous, intraperitoneal, intradermal, intramuscular) as recommended by RIBI on days 0 (200 μg MAPS), 28 (100 μg MAPS), 71 (50 μg MAPS), and 225 (50 μg of linear 5-MAPS or 17 μg for loop 5-MAPS). The rabbits were bled on days 0, 28, 38, 44, 71, 82 (week 12), 89, 225, and 235 (week 34).

ELISA Titers. Titrations of rabbit antisera against linear 5, loop 5, and rgp120 were carried out in duplicate, and the results were averaged. Background absorption was determined by titrating each antiserum in the same manner but without antigen.

Linear 5/C and loop 5/C (Table 1) were conjugated to biotin-BMCC (Pierce) according to the manufacturer. Bio-

tinylated-peptide (10 ng/100 μL of PBS/well) was added to 96-well neutrAvidin coated microtiter plates (Pierce) for 2 h at room temperature which were then washed four times with distilled water. Rabbit antisera was serially diluted 2-fold with 1% BSA/0.05% Tween 20/PBS into titer wells and incubated for 1 h at 37 °C. After washing 10 times with distilled water, bound antibody was determined using alkaline phosphatase-conjugated goat antirabbit IgG F(ab′)$_2$ (Pierce) [100 μL/well of 1/500 dilution of IgG F(ab′)$_2$ in 1% BSA/0.05% Tween 20/PBS]. After incubation at 37 °C for 1 h and washing 10 times with distilled water, 100 μL of developing solution (1 mg of pNPP/mL of developing buffer) was added. The developing solution was prepared by adding 5 mg of pNPP (Sigma) to 5 mL of developing buffer (50 mL of diethanolamine, 50 mg of $MgCl_2 \cdot 6H_2O$, and 97.5 mg of NaN_3 were brought to 500 mL, pH 9.7, with ddi·H_2O and NaOH). Optical density was determined at 415 nm after 30 min with a Molecular Devices SpectraMAX 190.

Titers to protein were determined using rgp120$_{MN}$ (ImmunoDiagnostics Inc.). High binding 96-well microtiter plates (Costar, polystyrene 1/2 area) were coated overnight at 4 °C with sheep PAb specific for the C-terminus of rgp120 (no. 6205, International Enzymes, Fallbrook, CA, 0.5 μg of PAb/50 μL of PBS/well). After removal of unbound antibody by washing four times with distilled water, rgp120 (0.05 μg of rgp120/50 μL of 1% BSA/0.05% Tween 20/PBS/well) was added and incubated at room temperature for 2 h. Unbound rgp120 was removed by washing four times with distilled water, antibody was added, and the assay was continued in the same manner as described above.

End-point titers are the highest dilution of antisera that gave >2× background absorbance. Midpoint titers of antibodies for rgp120 are equal to the dilution of antisera that gave an optical density of 1.0 after correcting for background.

Competition ELISA Assay. Each experiment was carried out in duplicate and the results were averaged. First, linear 5/C-biotin (10 ng/well) or rgp120 (0.025 μg of rgp120/well) were bound to titer wells as described above. A subsaturating concentration of antibody was premixed with 4-fold serially diluted competing peptide and transferred to the antigen-coated wells (50 μL/well in 1% BSA/0.05% Tween 20/PBS). After incubation at 37 °C for 1 h, the unbound antibody was removed by washing 10 times with distilled water. Quantification of the bound antibody was carried out with alkaline phosphatase-conjugated goat antirabbit IgG as described above. 100% binding to plate-adsorbed antigen was determined in the absence of competing peptide. Background absorbance was determined without plate-adsorbed antigen and subtracted from the average of values with rgp120.

Neutralization Assays. Neutralization assays were carried out in triplicate in 96-well tissue culture plates (Costar). In a typical assay, 100 $TCID_{50}$ virus (MN or JR-CSF) was mixed with 2-fold serially diluted rabbit antisera or MAb in 100 μL of culture medium and incubated for 1 h at 37 °C. Then either 2×10^4 human T-lymphoid H9 cells (to MN) or 5×10^4 phytohaemagglutinin-stimulated, peripheral blood mononuclear cells (to JR-CSF) were added to each well and incubated for 24 h at 37 °C; PBMCs were pooled from three donors. After washing three times with culture medium and bringing each well to 200 μL with culture medium, incubation was continued for 7 days at 37 °C under 5% CO_2. Then 90 μL from each well was mixed with 10 μL of 10% empigein (Calbiochem, La Jolla, CA) and assayed for p24 in an ELISA (*38*). Reported values from the ELISA are based on median values from the triplicate determinations for each concentration of antibody.

NMR Spectroscopy. Peptides were dissolved in 0.5 mL of 10% D_2O/90% H_2O (v/v) and adjusted to pH 5.0 with aqueous NaOH and HCl solutions. Dioxane was added as an internal chemical shift reference (3.75 ppm). 1D and 2D COSY, P. E. COSY, TOCSY, and ROESY experiments were carried out with a Bruker AMX 500 spectrometer. 1D NMR spectra were run with presaturation of water. 2D ROESY spectra were run in the phase-sensitive mode using TPPI for quadrature detection in f_1. Typically, 32 transients of 1024 data points were acquired in the f_2 dimension at a spectral width of 5555 Hz with 512 t_1 increments which were zero filled to 2024 data points. A 400-ms mixing time was used. Additional ROESY spectra were acquired for loops 5 and 7 at 10 °C using a Bruker DRX-600 MHz spectrometer at a spectral width of 7186 Hz using eight transients for each of 512 increments and a 400-ms mixing time. Temperature coefficients were obtained from a series of 1D spectra. Probe temperatures were determined using a methanol standard. 1D and 2D data were processed and analyzed on a Silicon Graphics Indigo2 Extreme computer using Felix (Molecular Simulations, Inc).

RESULTS

MAb 58.2. MAb 58.2 was generated by White-Scharf et al. (*30*) to a 40-residue MN peptide (RP70) that encompassed the V3-disulfide loop. It was the most potent neutralizing MN MAb among >3000 V3 positive hybridomas (from 85 mice) generated by the peptide. MAb 58.2 also weakly neutralized primary isolates (*30*). MAb 58.2 is about twice as potent against MN as MAb 50.1 from the same series (*30*) that has been grouped with the most potent MN neutralizing human V3 MAbs (*39*). Although MAb 58.2 is technically an antipeptide MAb, its high potency suggested that it bound the MN V3 epitope in a conformation that could be used to represent the native structure.

Several approaches have been taken to characterize the MAb 58.2 epitope (*21*, *30*, *40*−*42*). Phage-displayed peptides and peptide arrays identified GPxR, the least variable region of the SND, as the core epitope (*40*). This specificity most likely accounts for the broad recognition of gp120s from primary isolates by MAb 58.2 (*41*). Alanine scanning of a RIHIGPGRAFY peptide with MAb 58.2 showed that it binds IGPGRAF (*30*). Later, serial deletion competition ELISAs indicated that MAb 58.2 binds RIHIGPGRAFY with the terminal amino acids contributing about 1000-fold to affinity (*42*).

A crystal structure of a Fab 58.2−Aib peptide complex showed that the antibody binds RIHIGPGR(Aib)FY (*21*). The bound structure (Figure 1) has been characterized as a strand followed by three overlapping β-turns (*21*). It can also be viewed in terms of a strand−β turn−pivot−β turn motif. Parsing the conformer in this manner identified structural elements that were useful for the design, manipulation, and conformational analysis of a mimetic. In this rendition, Fab 58.2 binds RIHI as a strand, and GPGR and R(Aib)FY as overlapping type I [$\alpha_R \rightarrow \alpha_R$] β-turns. Both β-turns are

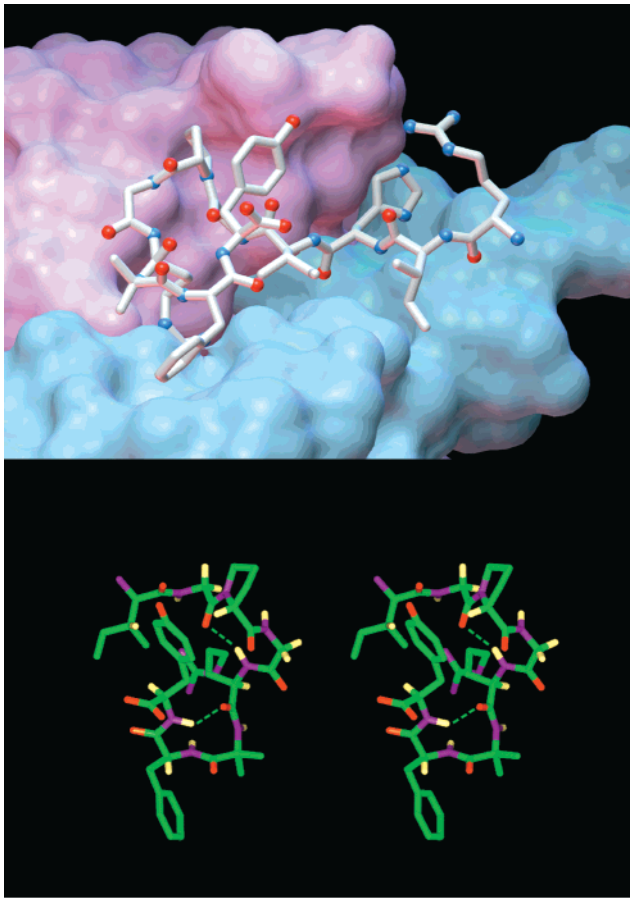

FIGURE 1: (top) Fab 58.2 bound MN V3 Aib-peptide, RHIGPGRAibFY (*21*), PDB accession code 1f58. V3 Aib-peptide (stick model) against a Connolly surfaced Fab 58.2 (light chain, pink; heavy chain, blue) as rendered by Mike Pique using AVS. (bottom) Stereoview of Fab 58.2 bound, IGPGR(Aib)FY.

Table 2: Comparison of the Conformations Adapted by GPGRAFY Peptides and Analogs in Aqueous Solution and Fab-Peptide Crystal Structures in Terms of a β-Turn−Pivot−β-Turn Motif

structure MN sequence	β-turn GPGR	pivot[a] R	β-turn RAFY
linear Aib-peptide NMR structure[b]	random coil	β	random coil[c]
loop 5 NMR structure[b]	type I	α[d]	type I
Fab 58.2-V3 Aib-peptide (*21*)	type I	β	type I
Fab 59.1-V3 peptides (*44*, *45*)	type II	α	type I
Fab 50.1-V3 peptide (*43*)	type II[e]	NB[f]	NB[f]

[a] Arg is shared by both β-turns and acts as a pivot occupying either the α- or β-region of Ramanchandran space. [b] From this study. Dynamic equilibria of structures including the indicated structures. [c] May include a minor population of β-turn. [d] It is likely that R also occupies the β-region, but overlapping NOEs precluded this assignment. [e] Densities for GP and part of G6 (ϕ angle) were detected and agree with a type II turn. [f] Not bound by Fab.

characterized by main-chain i, i + 3 hydrogen bonds and share Arg that acts as a pivot to orient the turns with respect to one another in a double-headed loop (Figure 1). This motif also provides a common framework for comparisons with the conformations of V3 peptides bound by two other MN neutralizing antibodies, Fabs 50.1 (*43*) and 59.1 (*44*, *45*) (Table 2), that are referred to in this study.

Design and Synthesis. Since a Fab 58.2-peptide crystal structure was not initially available, we began with a hypothetical structure based on a secondary structure prediction made by LaRosa et al. (*22*) who predicted that the V3

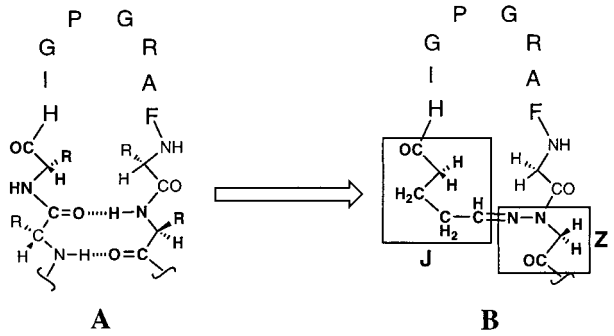

FIGURE 2: Transformation of a predicted MN V3 β-hairpin structure (A) into a hydrazone-linked loop 1 (B). The hydrazone link (boxed areas) was formed in a reaction between J and Z (Scheme 1).

sequence would form a β strand−type II β turn−β strand−α helix with GPGR occupying a type II turn. One manifestation of this prediction would place the SND in a β-hairpin. It was recently reported that a related V3 IIIB peptide binds a IIIB neutralizing MAb as a β-hairpin (*46*). β-hairpins are characterized by various sized loops at their apexes and a stem (*47*). The stems consist of antiparallel β-strands that hydrogen bond across alternating pairs of amino acids. The hydrogen bonds provide sites for substitution with the hydrazone link (*19*). For example, a predicted β-hairpin for the V3 MN sequence that includes the SND and a pair of hydrogen bonds characteristic of a stem is shown in Figure 2. The hydrazone link can be used to replace i + x → i main-chain hydrogen bonds in the manner shown for this structure to give in this case, loop 1 (Figure 2). However, the initial pair of hydrogen bonds could traverse a different set of amino acids determined by the size and position of the loop.

A set of corresponding linear and cyclic peptides was synthesized beginning with linear 1 and loop 1 (Table 1 and below). Loop 1 was then expanded using enhanced affinity for MAb 58.2 to identify a complementary loop while limiting as far as possible the composition of the loop to the SND. Corresponding linear and cyclic peptides were used to assess the effect of cyclization on affinity, independent of changes in amino acids. The hydrazone-linked peptides were synthesized on Rink amide resin using manual and machine-assisted multiple peptide synthesis according to Scheme 1. The coupling of Fmoc-amino acids to Z requires the use of an Fmoc-amino acid chloride since the reaction is sterically hindered (*19*). Fmoc-Gly chloride was used for coupling to Z for this series. Coupling to Z is not necessarily restricted to Gly (*19*). It required little more effort to assemble a hydrazone-linked peptide than a linear peptide and the yields were high for cyclic peptides of this complexity. Individual amino acids and their replacements are referred to using the numbering system in Table 1.

Peptide Affinities. The affinities of linear and cyclic peptides for MAb 58.2 were determined using a competition ELISA assay (Figure 3) and are reported as affinity indices, EC_{50} values of the peptides relative to the EC_{50} value for linear 1 (Table 3). Assays were carried out at 37 °C to simulate the conformational differences that occur at physiological temperature.

Loop 1 bound MAb 58.2 with an affinity index of 23. A Fab 58.2−loop 1 crystal structure has been reported (*21*). The propylene moeity of the hydrazone link appears fully

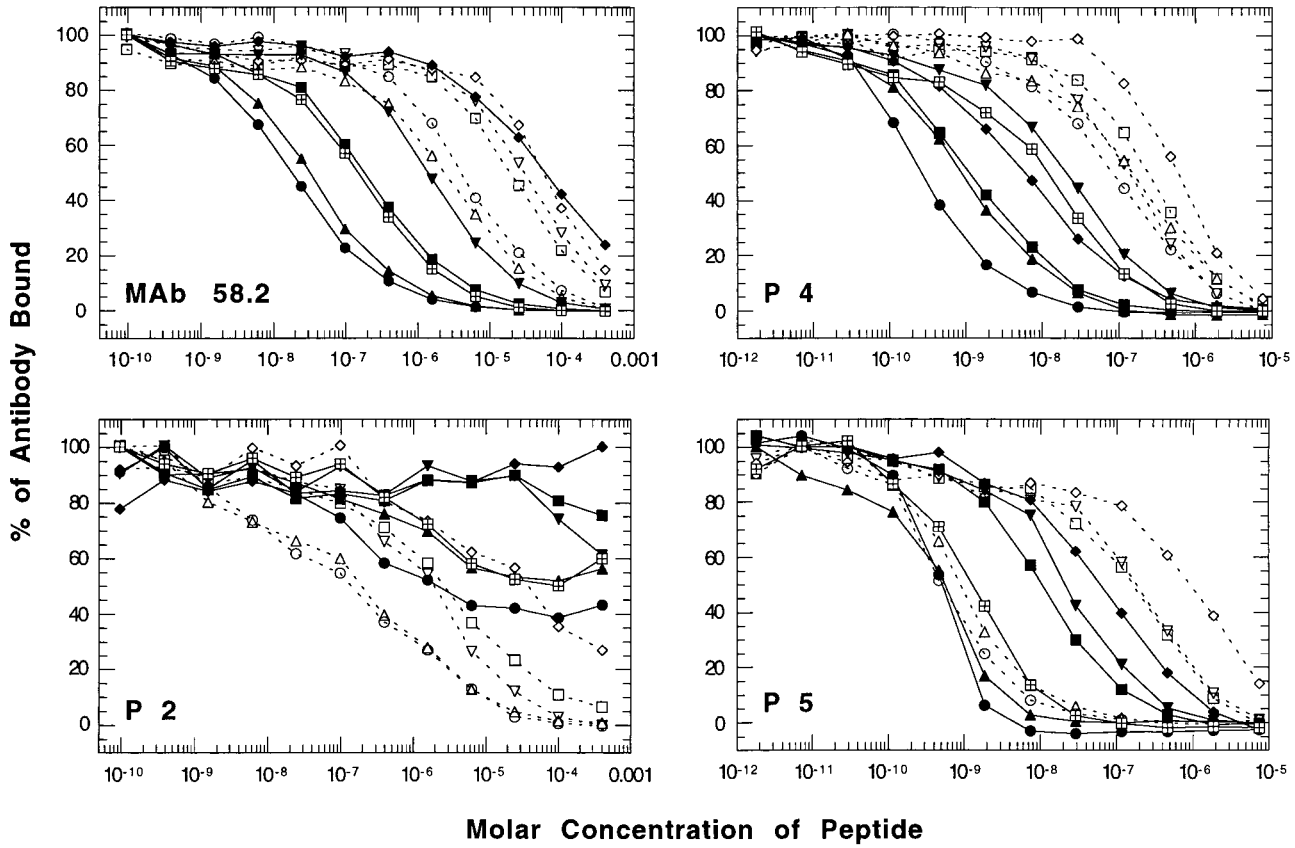

FIGURE 3: Competition ELISA assays of linear (1, ▽; 2, □; 3, ◇; 4, △; 5, ○) and loop peptides (1, ▼; 2, ■; 3, ♦; 4, ▲; 5, ●; 6, square with cross) for MAb 58.2 and rabbit antisera P2 (anti-linear 5), P4 and P5 (anti-loop 5). Peptides compete with plate-bound rgp120 (MAb 58.2, P4, P5) or linear 5 (P2). Percent antibody bound refers to the antibody bound by the plate-bound antigen. The peptides are identified in Table 3 which also includes relative EC_{50} values from these data.

Table 3: Affinity Indices of Linear and Loop Peptides for MAb 58.2 and P4 and P5 rgp120-Specific Antibodies[a]

peptide	sequence	MAb 58.2	P4	P5
linear 1	Ac-GHIGPGRAFGGG-NH_2	1.0	1.0	1.0
linear 2	Ac-GHIGPGRAFGGGG-NH_2	1.5	0.6	1.2
linear 3	Ac-GHIGP(D-Ala)RAFGGGG-NH_2	0.3	0.2	0.2
linear 4	Ac-GHIGPGR(Aib)FGGGG-NH_2	13	1.0	222
linear 5	Ac-GHIGPGR(Aib)F(D-Ala)GGG-NH_2	10	1.4	400
loop 1	[JHIGPGRAFGZ]G-NH_2	23	6.5	9.5
loop 2	[JHIGPGRAFGGZ]G-NH_2	167	108	20
loop 3	[JHIGP(D-Ala)RAFGGZ]G-NH_2	0.5	22	3.3
loop 4	[JHIGPGR(Aib)FGGZ]G-NH_2	968	144	370
loop 5	[JHIGPGR(Aib)F(D-Ala)GZ]G-NH_2	1667	464	400
loop 6	Ac-[CHIGPGR(Aib)FGGC]-NH_2	176	11	167

[a] Affinity indices are reciprocals of the (EC_{50} values for the peptide)/(EC_{50} value for linear 1). The EC_{50} values were obtained from Figure 3.

extended in the Fab 58.2 bound structure suggesting that loop 1 is barely wide enough to fit the binding site. This impression was strengthened by the later observation that Gly10 in loop 1 was rotated relative to Tyr10 in the Fab 58.2 bound linear Aib-peptide (Figure 1). When loop 1 was expanded by adding a second Gly to the C-terminal end of the SND to give loop 2, the affinity index improved to 167. We therefore eliminated smaller loops from consideration. When loop 1 was instead expanded from the N-terminus by adding Ileu to give [JIHIGPGRAFGZ]G-NH_2, the affinity index remained at about 23 (not shown). Since the higher affinity index for loop 2 suggested considerable complementarity with the MAb 58.2 binding site, ring expansion was stopped to limit the mimetic as far as possible to the SND. For comparison, MAb 58.2 binds RP70 (complete MN V3 disulfide loop peptide) with 22-fold higher affinity than an MN linear peptide that encompasses the complete MAb 58.2 epitope (*42*).

Three additional modifications were made to loop 2 at the **X** positions, [JHIGP**X**R**X**F**X**GZ]G-NH_2, to either probe conformational preference and/or improve the affinity of loop 2 for MAb 58.2. (i) Since Fab 58.2 binds GPGR as a type I turn (Figure 1), loop 3 was prepared with a Gly6/D-Ala substitution as a potential probe for this preference. D-Ala at the i + 2 position of a β-turn in cyclic pentapeptides destabilizes the type I turn and favors the type II turn (*48*). The affinity index for loop 3 decreased from 167 to 0.5 indicating the difficulties of binding GP(D-Ala)R as a type I turn. An examination of the Fab 58.2−peptide crystal structure (Figure 1), indicated that the D-Ala α-methyl group would not interfere sterically if loop 3 were bound as a type I turn. Consequently, loop 3 provides a sensitive probe for

type I turn specificity. (ii) Fab 58.2 also binds R(Aib)FY as a type I turn (Figure 1). Aib favors the α_R-region of Ramachandran space (*49*) which is adopted by Aib8 ($\phi = -50°$, $\psi = -42°$) in the Fab 58.2 bound peptide (*21*). The additional α-methyl group on Aib (as compared with Ala) projects into space and does not contact Fab 58.2 in the crystal complex (Figure 1). When Ala8 in loop 2 was replaced with Aib to give loop 4, the affinity index improved about 6-fold to 968 indicating a conformational stabilization by Aib. (iii) The conformational preference of MAb 58.2 for Gly10 was probed. Gly is a preferred amino acid at the i, i + 3 position of type I turns, often occupying the α_L-region of Ramachandran space (*59*). Consequently, it is not surprising to find that D-amino acids can occupy i, i + 3 positions in type I turns in cyclic pentapeptides (*48*, *50*). When Gly10 was substituted with D-Ala to give loop 5, the affinity index improved to 1667. However, when D-Ala10 in loop 5 was replaced with Aib, the replacement had little effect on affinity (not shown) suggesting that X10 can occupy different regions of Ramachandran space in the bound state.

A disulfide loop 6 (Table 1) was prepared to determine the effect of a different linker on affinity. Disulfide links are often found just beyond β-strand pairs where they are offset diagonally from the strands (*51*). The disulfide loop 6 links cysteine side chains to form a 38-member ring while the hydrazone-linked loop 5 is a main-chain linked 37-member ring. Replacing the hydrazone link with the disulfide link reduced the affinity index of loop 6 for MAb 58.2 to 176 (Figure 3) suggesting that the hydrazone link can better accommodate the conformer bound by MAb 58.2 than the disulfide link.

The affinities of linear and loop peptides for a second V3 MAb 59.1 were compared to determine whether MAb 59.1, which binds peptides in a related but different conformation to MAb 58.2 (Table 2), could discriminate among these peptides. MAb 59.1 bound loops 2 and 4 with about 4-fold higher affinity than the corresponding linear 2 and linear 4 peptides (not shown). The substitution of Aib for Ala8 had little or no effect on affinity. Consequently, loop 5 stabilizes or can adapt to the MAb 59.1 bound conformer but not nearly as well as to the conformer bound by MAb 58.2.

One further comparison was made of the affinity of MAb 58.2 for the MN peptide, acetyl-RIHIGPGRAFY-NH_2, with a corresponding peptide, acetyl-SIHIGPGRAFY-NH_2, representative of the primary isolates that were weakly neutralized by the antibody (*30*). A competition ELISA assay showed that MAb 58.2 bound the MN peptide with 14-fold higher affinity than the primary isolate peptide (Supporting Information). The N-terminal Arg forms a bifurcated, electrostatic bond between the guanidinium side chain and an aspartyl carboxylate group on the Fab (Figure 1) that likely accounts for the higher affinity of the MN peptide.

NMR Structural Studies. The high affinity indices of loops 2, 4, 5, and 6 for MAb 58.2 (Table 3) suggested that these cyclic peptides adopted conformation(s) in water that mimicked the MAb 58.2 bound conformer to a much better degree than the linear peptides. To assess this possibility, NMR structural studies were carried out on loop 5 and compared with those for a linear V3 Aib-peptide, acetyl-GHIGPGR(Aib)FGGG-NH_2, in 10% D_2O/H_2O, pH 5.0, at or near ambient temperatures.

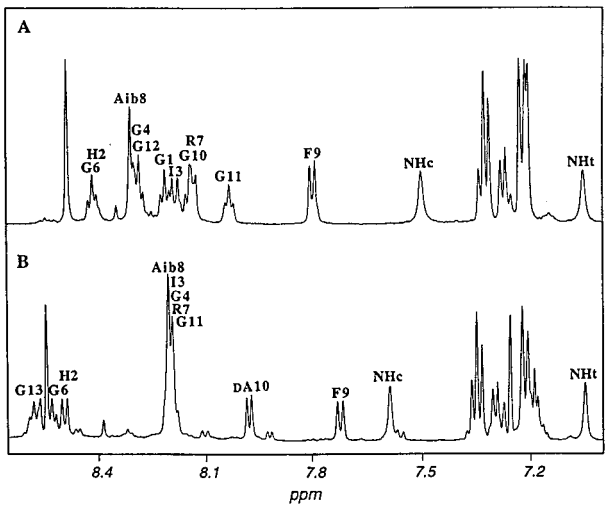

FIGURE 4: The amide proton region of 1D NMR spectra for (A) 20 mM linear Aib-peptide, acetyl-GHIGPGR(Aib)FGGG-NH_2, in 10% D_2O/90% H_2O at pH 5.0, 24 °C and (B) 20 mM loop 5 at pH 5.0, 21 °C, in 10% D_2O/90% H_2O.

A comparison of the amide NH regions of 1D NMR spectra for the linear Aib-peptide and loop 5 (Figure 4) revealed large shifts in resonance positions indicating major differences in chemical environment and conformation consistent with a structural basis for affinity enhancement. Both the linear and cyclic peptides showed a minor component (10%) that could arise from cis−trans isomerization at the Gly−Pro tertiary amide link. Another short, protected MN V3 peptide has been reported to isomerize in DMSO (*52*). As expected, the major component of loop 5 displayed a strong $G4^{\alpha}$-$P5^{\delta}$ NOE indicating a trans peptide bond (*53*). Fab 58.2 binds V3 peptides with Gly−Pro in the trans configuration (Figure 1) (*21*). Although we could not establish full connectivities for the 10% isomer, a $G4^{\alpha}$-$P5^{\alpha}$ NOE was evident for a minor component in loop 5 (not shown) indicating the presence of a cis Gly−Pro isomer (*53*). The acylhydrazone is another potential source of cis−trans isomerization. No G^{α}-Z^{α} NOE was apparent for the major component indicating that the main-chain C−N link is in the trans configuration relegating the -N−N- link to the "cis" position. Fab 58.2 binds loop 1 in this configuration (*21*). Loop 5 showed additional minor components (<5%) (Figures 4 and 6), which may reflect isomerization at the acylhydrazone or the presence of minor peptide impurities, possibly from racemization since no impurities were detected by mass spectroscopy (Supporting Information).

Further structural information was developed for the linear Aib peptide and loop 5 major components. The resonance positions for all protons for the linear Aib-peptide and loop 5 were assigned (Supporting Information) from 2D-NMR experiments using standard sequential assignment methods (*54*). These include stereospecific assignments for the loop 5 F9 β-methylene protons (Figure 5 and Supporting Information) which were made according to the method of Basus (*62*).

The overlap of several resonances for main-chain amide protons for loop 5 (Figure 4) prompted the synthesis of loop 7 (Ileu3 to Val3) which led to a small improvement in resonance separation (Supporting Information). Loop 7 showed a similar set of minor components. ROESY experiments for loops 5 and 7 displayed the same structure-defining

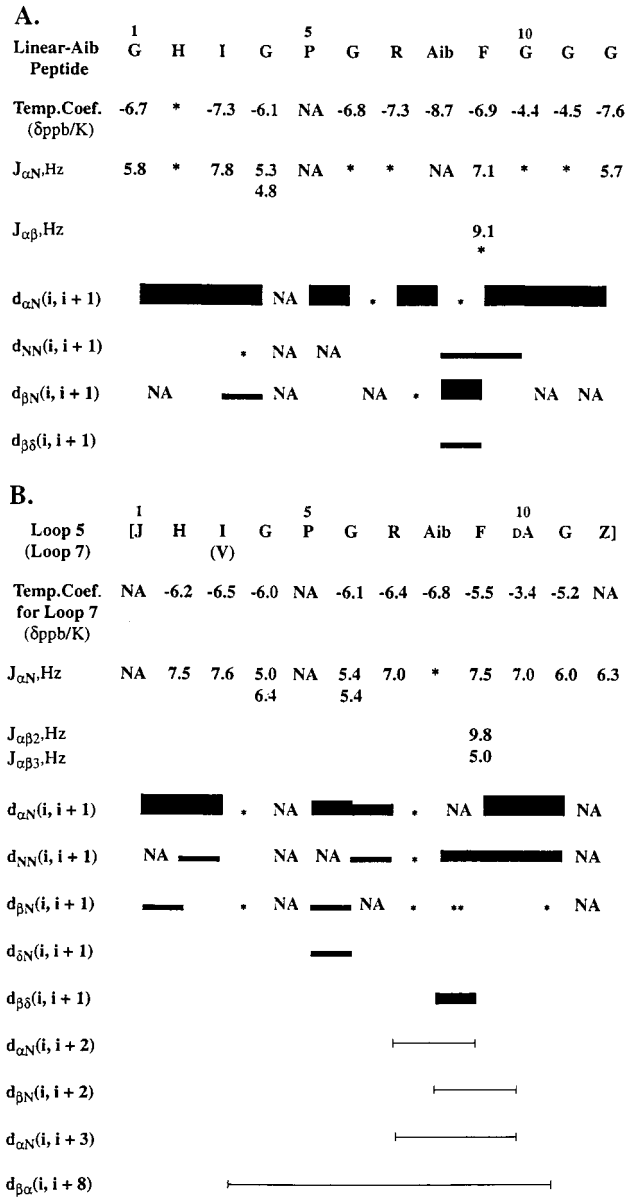

FIGURE 5: Summary of NMR data for the (A) linear Aib-peptide at pH 5.0, 24 °C and (B) loop 5 at pH 5.0, 21 °C. Temperature coefficients for loop 7 are included with the data for loop 5. Temperature coefficients were determined from linear regression analysis of five measurements made between 13−34 °C with $R > 0.996$ (Supporting Information). $J_{\alpha N}$ and $J_{\alpha\beta}$ were determined from 1D and P. E. COSY spectra. Asterisk (*) indicates overlapping signals. Double asterisks (**) indicate that both Aib8$^{\beta}$-F9^{N} NOEs were medium intensity. Strong, medium-strong, medium, and weak NOEs are indicated by the heights of the filled bars. Lines are for weak NOEs except for the Aib8$^{\beta}$-(D-Ala)10^{N} NOE which was medium intensity. Blank spaces, no NOEs; NA, not applicable. The loop 5 F9$^{\beta 2}$ which resonates at 2.95 ppm showed a strong F9$^{N\beta 2}$ NOE (Figure 6) and a weak F9$^{\alpha\beta 2}$ NOE (not shown), while F9$^{\beta 3}$ at 3.22 ppm showed a weak F9$^{N\beta 3}$ NOE (Figure 6) and a medium F9$^{\alpha\beta 3}$ NOE (not shown).

NOEs (Supporting Information) indicating similar structures. The affinities of loop 5 and 7 for MAb 58.2 differed by no more than 2-fold consistent with similar structures (Supporting Information). Since loop 5 and loop 7 are chemically and structurally very similar, the additional NMR data for loop 7 resulting from better separation of resonance positions are used to supplement the data for loop 5.

Secondary structures display characteristic NOE patterns (*53*), which along with other data can be used to identify

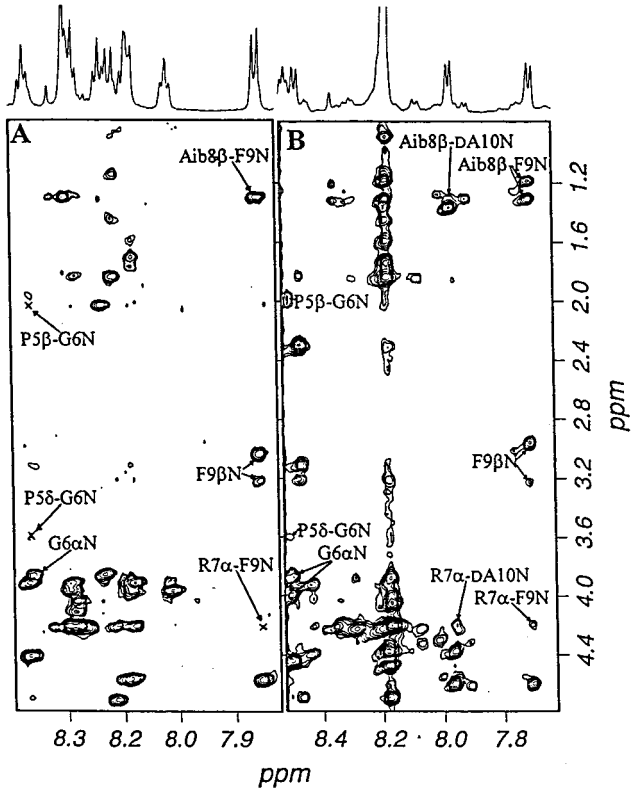

FIGURE 6: Portions of ROESY spectra for 20 mM solutions of (A) the linear V3 Aib-peptide, acetyl-GHIGPGR(Aib)FGGG-NH_2, in 10% D_2O/H_2O, pH 5.0, at 24 °C and (B) loop 5 in 10% D_2O/H_2O, pH 5.0, at 21 °C. NOEs that are indicative of β-turns are displayed by loop 5 but not by the linear Aib-peptide (x).

peptide conformations (*55*). The coupling constants, amide proton temperature coefficients, and NOEs for the linear Aib-peptide and loop 5 are summarized in Figure 5. Portions of spectra from 2D ROESY experiments identifying NOEs for the linear Aib-peptide and loop 5 are compared in Figure 6. Both peptides showed strong $d_{\alpha N}(i, i + 1)$ NOEs that are characteristic of unfolded forms (*55*). However, loop 5 displayed additional NOEs that indicated the stabilization of significant populations of β-turns within GPGR(Aib)F-(D-Ala).

Loop 5 showed P5$^{\delta}$-G6^{N}, P5$^{\beta}$-G6^{N} (Figure 6 and Supporting Information), and G6^{N}-R7^{N} (not shown) NOEs that were not observed for the linear Aib-peptide. In addition, the P5$^{\alpha}$-G6^{N} NOE for loop 5 was not as strong as for the linear peptide. These observations suggest that loop 5 stabilizes a type I β-turn at GPGR (*53*, *57*, *58*). The resonances for the G6 α-protons on loop 5, unlike those for the linear-Aib peptide, are separated (Figure 6) providing another indication of a better defined environment. Consequently, the $J_{\alpha N}$ coupling constants (5.4 Hz, 5.4 Hz) for the G6 α-protons may be significant. These coupling constants are, however, closer to those predicted for a type II turn (5 Hz) and a random coil (6.5 Hz) than a type I turn (9 Hz) (*58*). The medium-strong P5$^{\alpha}$-G6^{N} NOE could reflect the presence of a type II turn as well as a random coil (*53*, *57*, *58*). Type I and II turns are often but not always characterized by i, i + 3 hydrogen bonds (*56*, *57*). The temperature coefficient for the R7 amide proton was lower for loop 7 (6.4 ppb/K) than for the linear Aib-peptide (7.3 ppb/K) consistent with an i, i + 3 hydrogen bond. However, the effect is small and may reflect other phenomena. In this regard, R7 and Gln, which

are highly conserved by HIV-1 at GPG(R/Q) (*3*), are also favored at this position in type II turns for their ability to form side chain interactions with the i amino acid that substitutes for main-chain i, i + 3 hydrogen bonds (*59*). MAb 59.1 binds GPGR in this manner (*44*, *45*). Although the NMR data suggests that loop 5 stabilizes GPGR as a type I turn, it is likely to be in equilibrium with less ordered conformers and possibly other turn types.

The NMR data suggests that loop 5 stabilizes a second β-turn at R(Aib)F(D-Ala) as well. The data for R(Aib)F(D-Ala) which are characteristic of helices and β-turns (*53*, *58*) are consistent with the presence of type I and III β-turns. The type III turn [$\alpha_R \rightarrow \alpha_R \rightarrow \alpha_R \rightarrow \alpha_R$] has been merged with and classified as a type I turn [$\alpha_R \rightarrow \alpha_R$] since in both cases the β-turn defining i + 1 and i + 2 amino acids occupy the α-region of Ramachandran space (*60*, *61*). However, a type III turn is also one turn of a 3_{10}-helix that is characterized by additional NOEs (*53*, *58*) that were observed for loop 5.

The NMR data for R(Aib)F(D-Ala) can be summarized as follows. (i) Sequential $d_{NN}(i, i + 1)$ NOEs for (Aib)F(D-Ala)G (not shown) are characteristic of helices and the type III turn (*53*, *58*). (ii) The $R7^{\alpha}$-$F9^{N}$ NOE is weak and of similar intensity to the $R7^{\alpha}$-(D-Ala)10^{N} NOE (Figure 6 and Supporting Information) suggesting a 3_{10}-turn, i.e., type III turn (*53*, *58*). It is very unlikely that these weak NOEs or the weak $P5^{\delta}$-$G6^{N}$ described above arise from minor components buried under major component resonances since they are observed at two different temperatures for loop 5—at 10 °C (Supporting Information) and 21 °C (Figure 6)—indicating the same temperature dependencies as the major component resonances. In addition, these NOEs were observed for loop 7 (Supporting Information). (iii) An $Aib8^{\beta}$-(D-Ala)10^{N} NOE is predicted for type I and type III turns and observed as an overlapping NOE (Figure 6) for one of the α-methyl groups on Aib8. This NOE is clearly resolved for loop 7 (Supporting Information). The resonances for the two α-methyl groups on Aib8 are well-separated for loop 5 as compared with the linear Aib-peptide (Figure 6) consistent with a more structured environment. The pattern of $F9^{\alpha\beta}$ coupling constants, $F9^{N\beta}$ and $F9^{\alpha\beta}$ NOEs, which are summarized in Figure 5 and the accompanying legend, indicate that the conformation of the F9 side chain is largely restricted to the g+ conformation (χ angle = −60°) (*62*), in agreement with the Fab 58.2 bound Aib-peptide (Figure 1) (*21*). (iv) The temperature coefficient for the D-Ala10 amide proton of loop 7 (−3.4 ppb/K) is low, which is consistent with its participation in a hydrogen bond to the R7 carbonyl oxygen atom that is characteristic of type I and III turns. The temperature coefficient for the D-Ala10 amide proton in loop 5 which is well-resolved (Figure 4) is similarly low (not shown). The NMR data for R(Aib)F(D-Ala) suggests a very substantial population of type I turns that may be embedded in and/or in equilibria with helical-like turns. The linear Aib-peptide may stabilize minor populations of similar structures as suggested by weak $d_{NN}(i, i + 1)$ NOEs (not shown) for AibFG and a lowered temperature coefficient for the G10 amide proton.

Overall, the NMR data for loop 5 is consistent with a dynamic equilibrium of structures that include regions of disorder and conformers that stabilize type I turns at GPGR and/or R(Aib)F(D-Ala) that are not as evident in the linear Aib-peptide. The enhanced affinity of loop 5 for MAb 58.2 which binds GPGR(Aib)FY as overlapping type I turns can thus be attributed to conformational stabilization. However, it remains unclear whether loop 5 stabilizes the precise conformation recognized by MAb 58.2 (Table 2) or whether further conformational adjustments are required for binding.

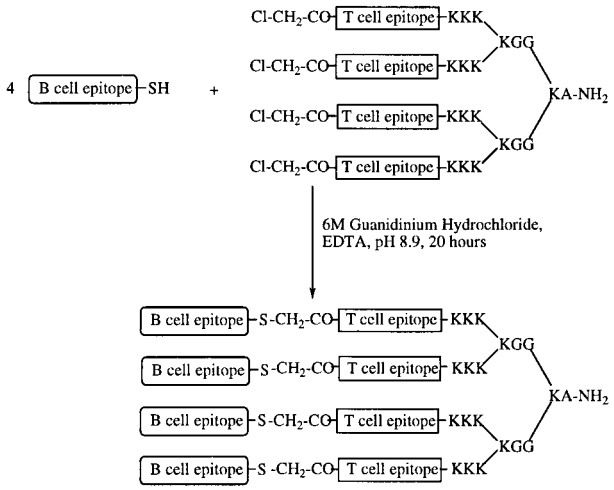

FIGURE 7: Synthesis of linear 5 and loop 5 MAPS. The B-cell epitope, either linear 5/C or loop 5/C, was reacted with a chloroacetylated T-cell epitope, QYIKANSKFIGITEL, on a MAPS core. The branch points were formed by coupling amino acids to the α- and ϵ-amino groups of Lys. Chemical structures are shown in Table 1 and Supplementary Information.

Immunogenicity. The corresponding linear 5 and loop 5 were incorporated into individual MAPS (Figure 7) for generating antibodies. The basic MAPS design (*35*) was modified by increasing the distance between branch points with tandem glycines (*36*) and inserting three tandem lysines at the carboxyl end of the four branches which imparts aqueous solubility (*37*). C-terminal cysteines on linear 5/C and loop 5/C were reacted with the chloroacetylated-tetanus toxoid T-cell epitope, QYIKANSKFIGITEL (TT2), on a four-branched MAPS core to give linear 5-MAPS and loop 5-MAPS (Figure 7). Chemical ligation opens a route to larger MAPS that can be synthesized with the purity required for characterization by MS (*63*). The TT2 epitope is capable of recruiting T-cell help in mice, rabbits, and humans (*64*, *65*). Both MAPS which are protein-sized (132 amino acids) were soluble in water and confirmed by MS (Supporting Information).

Two groups of three female NZW rabbits were immunized four times during the course of 34 weeks with linear 5-MAPS (rabbits P1−P3) and loop 5-MAPS (rabbits P4−P6) in RIBI's adjuvant (*66*). Dosage was minimized and the immunization schedule was lengthened to favor high affinity antibodies (*67*). High titers of antibodies to the immunizing peptide were observed following the third (12 week) and fourth (34 week) immunizations. Unless otherwise noted, analyses were carried out with the 12-week antisera.

The immunized rabbits showed striking differences in their antibody responses to the linear 5-MAPS and loop 5-MAPS (Figure 8). Each rabbit immunized with the loop 5-MAPS developed antibodies that bound rgp120, while rabbits immunized with the linear 5-MAPS did not (Figure 8 and Supporting Information). Both sets of rabbits developed high end-point titers (≥ 64 000 for the immunizing peptide) of antibodies that bound linear 5 and loop 5. However, while

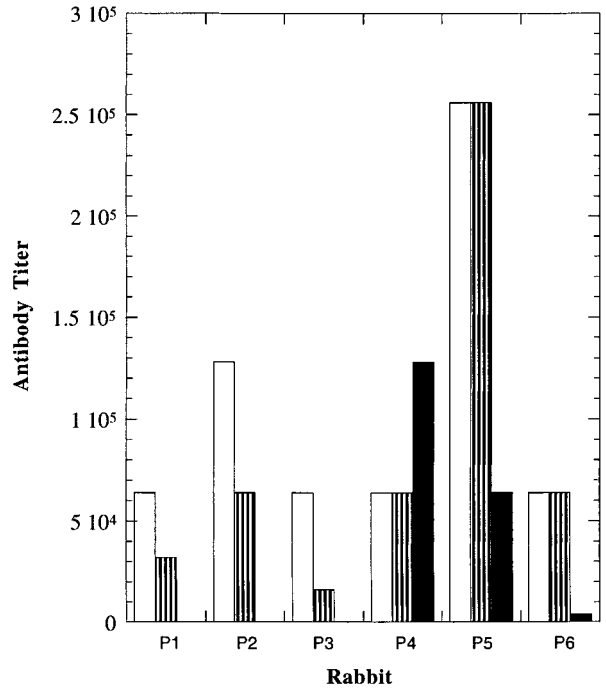

FIGURE 8: End-point titers of antibodies generated by rabbits P1−P3 (linear 5 MAPS) and rabbits P4−P6 (loop 5 MAPS) to linear 5 (clear), loop 5 (striped), and rpg120 (solid).

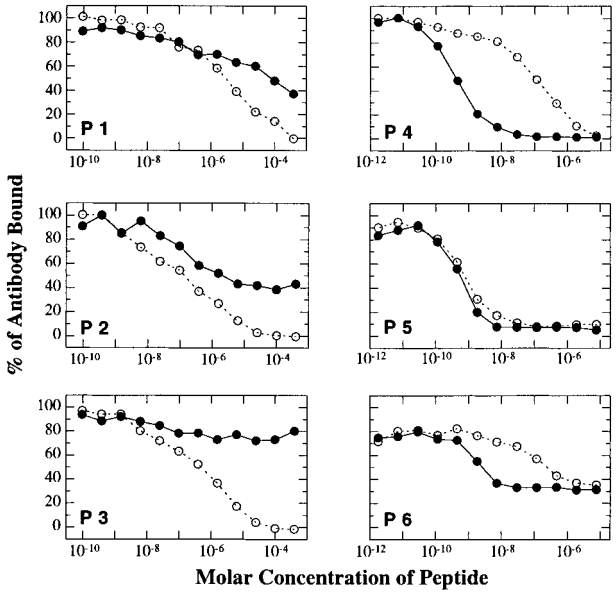

FIGURE 9: Competition ELISA assays of linear 5 (○) and loop 5 (●) for rabbit P1−P6 antibodies. Peptides compete with plate-bound linear 1 (P1−P3) or rgp120 (P4−P6). % Antibody bound refers to the antibody bound to the plate-bound antigen. The data for P2, P4, and P5 are from Figure 3.

the titer profiles for rabbits immunized with the linear 5-MAPS were similar, those immunized with the loop 5-MAPS showed distinct differences. P4 antisera showed higher titer to rgp120 than to linear 5 and loop 5. P5 antisera showed very high titers to linear 5 and loop 5 and relatively lower titer to rgp120. P6 antisera showed high titer to linear 5 and loop 5 and very low titer to rgp120.

The antisera were further evaluated in competition ELISA assays. The relative affinities of linear 5 and loop 5 for P1−P6 antibodies were compared (Figure 9). Since the P1−P3 antisera did not bind rgp120, a C-terminal biotinylated linear 5 peptide was adsorbed to neutrAvidin coated titer wells for competition ELISAs with P1−P3 antisera. The P1−P3 anti-linear 5 antibodies bound linear 5 with higher affinities than loop 5. A significant fraction of the P1 and P2 antibodies bound loop 5, while P3 antibodies showed a smaller population of antibodies binding loop 5. The competition curves for P1 and P2 are relatively flat reflecting heterogeneous populations of antibodies.

Competition ELISAs for the P4−P6 antibodies was carried out on plate-bound rgp120 to characterize the protein-reactive antibodies. The rgp120-binding P4−P6 antibodies showed very high affinities for loop 5 [$EC_{50} = (0.5-2) \times 10^{-9}$ M^{-1}, Figure 9]. The EC_{50} values are at least 10-fold lower than that shown by MAb 58.2 for loop 5 ($EC_{50} = 2 \times 10^{-8}$ M^{-1}, Figure 3). Also, the EC_{50} values for loop 5 for the P4−P6 antibodies are about 100−1000 times lower than the EC_{50} values for linear 5 for the P1−P3 antibodies [$EC_{50} = (0.2-2) \times 10^{-6}$ M^{-1}]. Although the P4−P6 rgp120-binding antibodies are heterogeneous, the individual antisera differed enough that distinctions can be drawn. The P4 antibodies showed the greatest similarity to MAb 58.2. P4 antibodies binds loop 5 with a 330-fold lower EC_{50} value than linear 5. In contrast, P5 antibodies bind loop 5 and linear 5 with very similar apparent affinities. The P6 rgp120-specific antibodies showed higher affinity for loop 5 but represent a minor population. The competition curves for P4−P6 are more nearly sigmoidal than those for P1−P3 indicating antibodies with similar affinities.

The preferences of P2 linear 5 antibodies and P4 and P5 rgp120-specific antibodies were compared with MAb 58.2 using full peptide scans (Figure 3). These scans provide a more complete picture of the differences in the responses of rabbits to linear 5 (P2) and to loop 5 (P4, P5) as well as animal-to-animal differences in the response to loop 5 (P4 vs P5). Relative EC_{50} values (affinity indices) for MAb 58.2, P4, and P5 rgp120-binding antibodies are compared in Table 3.

The P4 rgp120-specific antibodies came closest to duplicating the competition profile for MAb 58.2 (Figure 3). The affinity indices were similar with those for loop 5 > loop 4 > loop 2 > loop 1 > linear 4/5 > linear 1/2 > linear 3 (Table 3) for both P4 antibodies and MAb 58.2. The P4 antibodies also bound the disulfide loop 6 with higher affinity than the corresponding linear 4 peptide implying a conformational effect independent of the linker. Loop 3 is the only peptide that strongly deviates from the general agreement. Whereas the substitution of D-Ala for Gly6 in loop 2 to give loop 3 decreased the affinity index 334-fold for MAb 58.2, it reduced the index about 5-fold for the P4 antibodies (Table 3). MAb 58.2 appears unique among the antibodies examined in its ability to strongly discriminate against loop 3.

The P5 rgp120-specific antibodies showed strong preferences for Aib-peptides that appeared to be nearly independent of whether the peptide was cyclized or not (Figure 3). The affinity index of P5 antibodies for linear 4 (Aib-peptide) was 185-fold higher than that for the corresponding linear 2 (Ala-peptide) (Table 3) implying that Aib was a core amino acid and that the additional α-methyl group on Aib was specifically bound by the P5 antibodies. The similar affinities and sharper competition curves of Aib-peptides for P5 antibodies may reflect very high affinity, stoichiometric binding, of Aib-peptides to these P5 antibodies. Although P5 antibodies

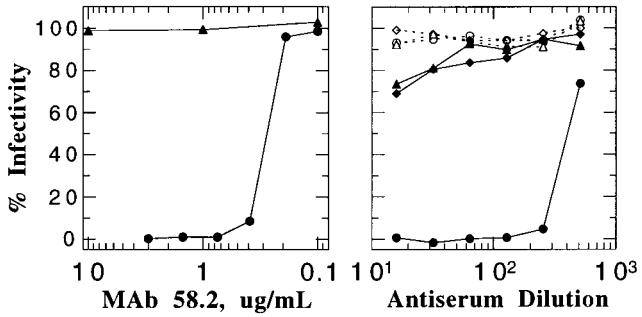

FIGURE 10: The neutralization of infection of H9 cells by 100 $TCID_{50}$ MN with (A) MAb 58.2 with (▲) and without (●) 41 μM loop 5 and (B) P1−P6 antisera, week 12 (P1, ○; P2, ◇; P3, △; P4, ●; P5, ♦; P6, ▲). The neutralization of MN by P4 antiserum is blocked by 41 μM loop 5 (not shown).

showed similar apparent affinities for linear and cyclic Aib-peptides, they showed a 17-fold higher affinity index for loop 2 (Ala-peptide) as compared with linear 2 (Ala-peptide). The higher affinity of gp120-reactive antibodies for a cyclic peptide was maintained, although it was not as great as observed for the P4 rgp120-specific antibodies (Table 3).

The P2 antibodies bound with higher affinities to linear peptides than to the corresponding cyclic peptides (Figure 3). The P2 antibodies showed about a 10-fold higher affinity index for linear Aib-peptides than for linear non-Aib peptides. Similar differences were observed for P1 and P3 antibodies (not shown). The apparent affinity enhancements of P1−P3 antibodies for linear Aib peptides (≈7−10-fold) were similar to MAb 58.2 (≈10-fold) suggesting a conformational effect. Regardless, Aib was not a core amino acid for most P1−P3 antibodies as it was for P5 antibodies (185-fold Aib effect). About half of the P2 antibodies bound loop peptides (Figure 3), while the remaining half did not. The inability to bind a loop could reflect conformational incompatibilities between anti-linear 5 antibodies and loops or it could reflect the requirement for a free N-terminal amino acid (wrap-around binding). However, at least a half of P1 and P2 antibodies and a quarter of P3 antibodies bound loop 5 in ELISAs (Figure 8) indicating that these antibodies do not require a free end and should not be limited by this requirement from binding rgp120.

The P4−P6 rgp120-binding antibodies share characteristics that were not found for the P1−P3 antibodies, namely, high affinities and a preference for cyclic peptides. Although the modified regions of the peptides could contribute to the affinity of rabbit antibodies for peptides (P5 antibodies for Aib), rgp120 is unmodified. The simplest interpretation of rgp120 binding is that the loop 5 antibodies are more compatible with the conformation of the V3 epitope on rgp120 than the linear 5 antibodies.

HIV Neutralization. Each of the rabbit antisera and MAb 58.2 were tested for the neutralization of MN infection of human T-lymphoid H9 cells (Figure 10). MAb 58.2 neutralized MN with $IC_{90} = 0.75$ μg/mL. P1−P3 linear 5 antisera had no effect on MN. The loop 5 P4 antiserum (12 week, 34 week) neutralized MN with titers of 128 and 100, respectively. P5 and P6 antisera (12 week) showed weak neutralizing activity at 1/16 antiserum dilution. Several controls were run concurrently. Neither preimmunization P4 serum, loop 5 alone (41 μM), MAb 58.2 mixed with loop 5 (41 μM), nor P4 antiserum (34 week) mixed with loop 5 (41 μM) neutralized MN.

Table 4: Antibody Midpoint Titers for rgp120, MN Neutralization Titers, and Potencies of MAb 58.2 and P1−P6 Antisera[a]

antibodies	rgp120 midpoint titer	neutralization titer IC_{90}	potency (rgp120 titer/ neutralization titer)
MAb 58.2	5.0×10^5	1.5×10^4	33
P1−P3 (12 week)	<125	<16	NA
P4 (12 week)	1.0×10^4	128	78
P4 (34 week)	1.0×10^4	100	100
P5 (12 week)	4.5×10^3	<16	>281
P6 (12 week)	200	<16	>13

[a] Antibodies are from 10-day bleeds following the third (12 week) and fourth (34 week) immunizations. rgp120 midpoint titers were determined from the reciprocols of MAb 58.2 (11 mg/mL) or antisera dilutions that gave an optical density of 1.0 in the standard ELISA (Materials and Methods). Neutralization titers are for reciprocols of the highest dilution of antibody that suppressed detectable levels of p24. Potencies are rgp120 midpoint titer/IC_{90}, neutralization titer. NA, not applicable.

Since a goal of this study was to determine whether the potent neutralizing activity of a template MAb could be recapitulated with a mimetic identified by the MAb, we compared the neutralizing potency of the rabbit antibodies with MAb 58.2 (Table 4). Potency is a measure of the concentration of an antibody required for neutralization. Since PAbs are complex mixtures of antibodies, we used midpoint antibody titer for rgp120/neutralization titer as a measure of potency (Table 4). These measures served two purposes. First, they provided a means for comparing the neutralizing activity of PAbs with a template MAb. Second, since the neutralization sensitivity of HIV-1 can vary (*68*, *69*), a MAb can provide a standard for wider comparisons.

MAb 58.2 and P4 antisera (12 week, 34 week) neutralized MN with similar potency (Table 4) indicating that loop 5 was capable of recapitulating the activity of MAb 58.2. Since MAb 58.2 compares favorably with the most potent V3 MAbs (see above), the P4 antiserum is also potent. On the other hand, the P5 rgp120-specific antibodies were less potent than MAb 58.2 (Table 4). The P6 rgp120-specific antibodies would have to be quite potent to account for even a weak neutralizing titer since they were generated at a far lower titer than the P4 and P5 rgp120-specific antibodies (Table 4).

Both MAb 58.2 and P4 antiserum were tested for the neutralization of JR-CSF, an HIV-1 primary isolate (*70*) that has proven refractory to other V3 MAbs (*71*). Although the JR-CSF V3 sequence, SIHIGPGRAFY, differs from the MAb 58.2 MN epitope, RIHIGPGRAFY, at the N-terminus of the MAb 58.2 epitope, MAb 58.2 weakly neutralized JR-CSF ($IC_{50} = 200$ μg/mL). This is in agreement with previous reports that MAb 58.2 weakly neutralized primary isolates (*30*). The neutralization of JR-CSF by MAb 58.2 was blocked by loop 5 (41 μM) indicating that neutralization was antibody-specific. Loop 5 (41 μM) by itself did not block infection. P4 antiserum (week 34) had no effect on JR-CSF infection at 1/4 dilution.

Clonal Selection. P4−P6 antibodies show very distinct characteristics indicating animal-to-animal differences in antibody responses to loop 5. First, the relative titers of P4−P6 antibodies to linear 5, loop 5, and rgp120 are distinctive (Figure 8). Second, the P4 and P5 rgp120-specific antibodies show clear differences in relative affinities for the same set

of linear and loop peptides in competition ELISAs (Figure 3). Third, P4 antiserum potently neutralized MN, while the P5 and P6 antisera were weakly neutralizing (Figure 10). These results imply a restricted clonal response of B-cells to loop 5 by the individual rabbits. The clearest case for clonal selection can be made with P5 rgp120-specific antibodies since they show a strong preference for the Aib-peptides. The Aib-peptides differ from the Ala-peptides by the addition of a single α-methyl group that represents about 1% of the mass of loop 5. However, most if not all of the P5 rgp120-specific antibodies show large affinity enhancements for the linear 4 Aib-peptide as compared with the corresponding linear 2 Ala-peptide (Figure 3). This implies that most of these P5 antibodies bind the extra methyl group suggesting that a very narrow population of rgp120-specific antibodies was generated by P5.

DISCUSSION

A striking result from the current study was the 5500-fold range of affinities of linear and loop peptides for MAb 58.2 (Figure 3). These affinity differences are most likely due to structural changes within the peptide rather than contributing or interfering interactions of modified regions of the peptide with MAb 58.2. The modifications were made exterior to the observed binding face of V3 peptides in Fab 58.2-peptide crystal complexes (*21*). The wide range of peptide affinities shows that the affinity of an antibody for a peptide can be extraordinarily sensitive to peptide structure.

Loop 5 binds >1000-fold more tightly to MAb 58.2 than the corresponding unconstrained V3 peptides (linear 1 and 2). Our literature search went back 27 years to the 17-residue disulfide loop of lysozyme to find a similarly large effect (*72*). The earlier study, as does the present one, proposed that the enhanced antigenicity and immunogenicity of the cyclic peptide was due to a conformational effect. This proposal was questioned for the lysozyme loop study (*73*) since no direct evidence was presented that the synthetic lysozyme loop adapted a native structure. The current study provides a structural analysis that supports a conformational basis for enhanced activity.

The relationship between the structure and affinity of a peptide for an antibody has been described by Anfinsen and co-workers (*12*). Formally, affinity can be viewed as the product of the fraction of the total peptide that is folded, reflecting K_{conf}, the equilibrium constant for folding, and the binding constant for the folded peptide. Anfinsen (*12*) calculated that K_{conf} for folding a 51-residue fragment of staphylococcal nuclease is 2×10^{-4} reflecting a 5000-fold affinity enhancement for the catalytically active form of the nuclease as compared with that of the inactive fragment for PAbs generated by the native protein (*12*). The >1000-fold improvement in affinity of loop 5 relative to the unconstrained V3 peptide for MAb 58.2 indicates that large affinity enhancements can extend to short constrained peptides (8-residues) as well. Whereas K_{conf} for the large nuclease fragment could reflect that for the reconstitution of a discontinuous epitope (topological assembly of amino acids distant in sequence), the latter result with loop 5 indicates that large effects can extend to continuous epitopes.

Since peptides are mostly disordered in aqueous solution (*11*), constraining peptides to mimic protein substructures would be expected to improve their affinities for native protein antibodies in many cases. Indeed, preliminary studies show that hydrazone-linked peptides designed to stabilize loops and α-helices detect antibodies in various antisera to different pathogens that go undetected with the corresponding unconstrained peptides (*74*, *75*). This has important implications since it suggests that the native protein antibodies that are most suited for serving as templates for synthetic vaccine development are being missed in screens with unconstrained peptides but can nonetheless be detected with constrained peptides because of their much higher affinities.

Loop 5 was also far more immunogenic than linear 5. This difference reflects structural differences in the peptides. Thus, the antibodies generated to linear 5 by the P1−P3 rabbits showed affinity preferences for linear peptides in comparison with loop peptides (Figures 3 and 9) indicating the difficulties of accommodating a loop structure. Neither could the P1−P3 antibodies bind rgp120 (Figure 8), despite exposure of the SND, implying that conformational incompatibilities prevented binding. On the other hand, the P4−P6 rabbits generated antibodies to loop 5 that bound rgp120 (Figure 8 and Supporting Information). These antibodies also bound loop peptides as well as or with higher affinity than linear peptides (Figures 3 and 9) demonstrating their capacity for binding a loop that also can account for why they bound rgp120.

The P4−P6 antibodies also neutralized MN (Figure 10), although with very different activities. Animal-to-animal differences in neutralizing activity generated by V3 peptides have been frequently observed (*23*−*25*, *27*, *76*). However, the bases for these differences have rarely been explored. In one study, a comparison of the amino acid specificities of antibodies in nonneutralizing and neutralizing IIIB antisera showed only minor differences (*24*). Consequently, the affinity profiles of P1−P6 antibodies for the linear and loop peptides (Figures 3 and 9) are striking for the differences they revealed.

Neutralizing titers are determined by the concentrations of neutralizing antibodies and their potencies. The concentrations of V3 antibodies were measured as titers for linear 5, loop 5, and rgp120 (Figure 8). Although titers were high to the immunizing peptide, the P4−P6 antisera showed quite different titers to rgp120. Added to this, the neutralizing potencies of the P4−P6 rgp120-specific antibodies also differed (Table 4). These measures together with the affinity profiles of the rgp120-specific antibodies (Figures 3 and 9) provide rationales that can account for differences in neutralizing activity.

The higher neutralizing titer of the P4 antisera was due to both the higher relative concentrations of P4 rgp120-specific antibodies (Figure 8) and their higher potencies (Table 4). The P4 rgp120-specific antibodies were similar in potency to MAb 58.2 (Table 4) demonstrating that the activity of a template MAb can be recapitulated with a PAb response. The P4 antibodies were also generated to a smaller MN epitope, HIGPGRAF, than MAb 58.2, which binds RIHIGPGRAFY. MAb 58.2 could derive a considerable affinity advantage (up to 1000-fold) from flanking amino acids (*42*) that cannot contribute to the affinity of P4 antibodies for MN. Thus the P4 response shows that potent neutralizing activity can also be focused onto a smaller epitope.

A comparison of the affinity profile of linear and cyclic peptides for the P4 rgp120-specific antibodies with the profile for MAb 58.2 showed strong similarities (Figure 3). This is consistent with similar fine structure and conformational specificities for the SND that could account for their similar potencies (Table 4). These profiles, however, also differ in some ways which as discussed below may reflect on requirements for neutralization via the SND.

The lower neutralizing titer of the P5 antisera relative to the P4 antisera was due more to the lower potency of the P5 rgp120-specific antibodies than to concentration differences (Table 4). It has been shown that the lowered potency of neutralizing MAbs for MN is synomynous with lower affinity for the virus (*79*). Differences in the affinity of antibodies for MN could arise from a number of sources, including differences in fine structure and conformational specificities as well as access to the epitope of the virus (*79*). The affinity profile of P5 rgp120-specific antibodies (Figure 3) shows a strong affinity enhancement for Aib-peptides (Table 3) compared with Ala-peptides, indicating that the added α-methyl group on Aib can contribute significantly to affinity. Consequently, the affinity of these P5 antibodies for MN could be suboptimal. The specificity of the P5 antibodies for Aib-peptides also indicates differences in the epitope recognized by P4 and P5 antibodies that could possibly lead to differences in accessibility to the MN epitope. Regardless, the observation that most if not all of the P5 antibodies show a specificity for Aib provides strong evidence for a very narrow population of P5 rgp120-specific antibodies.

The P6 antisera showed, as did the P5 antisera, lower neutralizing titer for MN (Figure 10). However, the bases for lower neutralizing titers of the P5 and P6 antisera differ. The P6 rgp120-specific antibodies were generated at a much lower titer than either the P4 or P5 rgp120-specific antibodies (Figure 8). Thus the lower neutralizing titer for P6 antisera reflects lower rgp120-specific antibody concentration rather than potency. The P6 rgp120-specific antibodies would have to be quite potent to account for even weak neutralizing titer (Table 4). The P6 rgp120-specific antibodies showed like the P4 antibodies a strong preference for loop 5 as compared with linear 5 (Figure 9) consistent with a similar conformational preference providing a basis for higher potency (Table 4). However, for the P6 rabbit, a third class of loop 5 antibodies predominated that bound both linear 5 and loop 5 but did not bind rgp120 (Figure 8).

The appearance of distinct populations of antibodies in the P4−P6 rabbits implies clonal selection and an amplification process. Amplification provides a mechanism for generating populations of antibodies with specificities for selected conformers or families of conformers. Jemmerson and Blankenfeld (*10*) showed that the activation of a B-cell for antibody generation is dependent on the immunogen achieving an affinity for the antigen receptor on the B-cell that exceeds that for binding the receptor, i.e., binding alone does not necessarily lead to antibody generation. The rgp120 specific antibodies generated by the P4−P6 rabbits showed much higher affinity for the corresponding immunogen, loop 5 ($EC_{50} \approx 10^{-9}$ M), than did the P1−P3 antibodies for linear 5 ($EC_{50} \approx 10^{-6}-10^{-7}$ M) (Figure 9), which may also be related to this phenomenon and the development of distinctive antibody populations.

The nonimmunogenicity of linear 5 was not entirely expected since other linear peptides with V3 sequences are immunogenic (*23*, *24*, *27*). For example, Vu et al. (*27*) reported that a long C4−V3 MN peptide (39-residues; 23 from V3) generated high neutralizing titers to MN in rhesus monkeys (2000 to >5000) which showed not only that the C4−V3 MN peptide is immunogenic but implies that it was more immunogenic than loop 5. However, comparisons are complicated for instance by differences in neutralization assays. The neutralization sensitivity of HIV-1 can vary widely for ostensibly the same assay (*68*, *69*). Also, longer peptides might generate neutralizing antibodies to epitopes other than the SND. MAb 58.2 served as a reference MAb in this study indicating that loop 5 generated potent neutralizing antibodies to the SND.

The difference in the immunogenicity of linear 5 and loop 5 is structure-based and indicates that a degree of conformational compatibility must be achieved for antibodies to bind the SND on MN. Structure-based rationales have also been proposed to account for the immunogenicity of long V3 peptides (*11*, *27*, *56*). Various NMR studies show that long V3 peptides stabilize structures at various positions in aqueous solutions at 5 °C (*27*, *56*, *77*). It has been suggested from models based on NMR data that the C4−V3 MN peptide stabilizes a contiguous apolar surface at I1−H2−I3−G4−P5 (our numbering) and noted that this structure correlates with neutralizing activity against MN (*27*). Long V3 peptides also stabilize β-turns at GPGR (*11*, *27*, *56*, *77*) that have been proposed to account for V3 peptide immunogenicity (*11*, *56*). Evidence for a β-turn at GPGR was dependent on the length of V3 peptides (*56*, *77*). Many factors including peptide length, copeptide (*24*, *27*), carbohydrate (*77*), or conjugate protein (*78*) could alter the balance between disorder and structure that in turn may determine V3 peptide immunogenicity.

The immunogenicity of loop 5 could be due to its general loop shape and/or the stabilization of β-turns at GPGR and R(Aib)F(D-Ala). This compares with observations that MAbs 58.2, 50.1, and 59.1 bind β-turns at these positions and also neutralize MN. However, the types of β-turns and their relative orientations differ for the MAb bound conformers (Table 2) (*21*). These differences occur largely at GPGR suggesting that GPGR is flexible enough on MN to accommodate these differences. This apparent flexibility could also account for why P4 rgp120-specific antibodies and MAb 58.2 neutralize MN with similar potencies yet show wide differences in their relative affinities for loop 3 (Figure 3). Loop 3 is less flexible at PG due to the G6/D-Ala substitution. Consequently, it could be used to distinguish differences in the conformational preferences of MAb 58.2 and the P4 antibodies for this position (Figure 3). PG on MN is presumably more flexible than P(D-Ala) on loop 3 since both the P4 antibodies and MAb 58.2 neutralize MN with similar potencies although they presumably bind PG on MN in different conformations.

It can be questioned as to whether the MAbs 58.2, 50.1, 59.1, and the P4 antibodies complement the native SND as well as they might. Although the V3 MAbs were selected for neutralizing potency, they are technically antipeptide antibodies that in general are not anticipated to faithfully mirror native protein structure. If this were the case, then one might expect to find human V3 MAbs generated to

native conformations that fit MN better and are more potent. However, MAb 50.1 (and by extrapolation, the similarly potent MAb 58.2 and P4 antibodies) was found to be more potent against MN (IC_{50} = 0.08 μg/mL) than many V3 human MAbs (IC_{50} = 0.05−5 μg/mL) in the same assay (*39*). One of these HuMAbs, MAb 391/95-D (*29*, *39*), binds the same MN sequence as MAb 58.2 (*42*). Thus the data suggest that GPGR can readily undergo conformational transition(s) on MN.

Overall, this study demonstrates the enormous effect that conformational restriction can have on the antigenicity and immunogenicity of a short, synthetic peptide. It shows the stability of the hydrazone link under physiological conditions and the effectiveness of the loop-MAPS at generating native protein reactive antibodies. It also makes evident the simplifying role that an antibody template can play in identifying and improving a constrained peptide immunogen using enhanced affinity as a measure of fit. The hydrazone link could find wider use since it can constrain peptides to α-helices (*19*) as well as loops that are among the more commonly found substructures on protein surfaces. The effectiveness of an HIV-1 vaccine will likely depend on the degree to which it can generate immune responses to neutralizing epitopes defined by constant amino acids while excluding dependence on variable amino acids. Constrained peptides provide a means for focusing antibodies on defined epitopes. A continuing use of constrained peptides can be expected to lead to improved strategies and further perspectives on synthetic and HIV-1 vaccine research.

ACKNOWLEDGMENT

We thank Dr. Al Profy for providing MAbs 58.2 and 59.1, Dr. Lin-chiang Chiang at NuMega Resonance Labs, San Diego, for NMR data collection, and Dr. James Tam for stimulating discussions.

SUPPORTING INFORMATION AVAILABLE

Tables of NMR chemical shift data for the linear V3 Aib-peptide and loop 5. HPLC chromatograms for the purification of loop 5 and loop 5-MAPS. Mass spectra of MAPS-core, linear 5-MAPS, loop 5, and loop 5-MAPS. Titration curves of linear 5 and loop 5 antisera for rgp120. Competition ELISAs indicated in the text. Plots for temperature coefficients for the linear V3 Aib-peptide and loop 7. Portions of 600 MHz 2D ROESY spectra for loops 5 and 7 at pH 5.0, 10 °C. This information is available free of charge via the Internet at http:/pubs.acs.org.

REFERENCES

1. Burton, D. R., and Moore, J. P. (1998) *Nat. Med. 4 (5)*, 495−498.
2. Parren, P. W. H. I., Moore, J. P., Burton, D. R., and Sattentau, Q. J. (1999) *AIDS 13*, S137−S162.
3. *Human Retroviruses and AIDS 1998: Compilation and Analysis of Nucleic Acid and Amino Acid Sequences*. (1998) (Korber, B., Kuiken, C. L., Foley, B., Hahn, B., McCutchan, F., Mellors, J. W., and Sodroski, J., Eds.) Los Alamos National Laboratory, Los Alamos, NM.
4. Pilgrim, A. K., Pantaleo, G., Cohen, O. J., Fink, L. M., Zhou, J. Y., Zhou, J. T., Bolognesi, D. P., Fauci, A. S., and Montefiori, D. C. (1997) *J. Infect. Dis. 176*, 924−932.
5. Zhang, Y-J., Fracasso, C., Fiore, J. R., Björndal, A., Angarano, G., Gringeri, A., and Fenyö, E. M. (1997) *J. Infect. Dis. 176*, 1180−1187.
6. Van Regenmortel, M. H. V. (1996) *Methods*, *9*, 465−472.
7. Sela, M., and Arnon, R. (1992) *Vaccine 10*, 991−999.
8. Sela, M., Schechter, B., Schechter, I., and Borek, F. (1967) *Cold Springs Harbor Symposium on Quantitative Biology 32*, 537−545.
9. Jemmerson, R. (1987) *Proc. Natl. Acad. Sci. U.S.A. 84*, 9180−9184.
10. Jemmerson, R., and Blankenfeld, R. (1989) *Mol. Immunol. 26*, 301−307.
11. Dyson, H. J., and Wright, P. E. (1995) *FASEB J. 9*, 37−42.
12. Sachs, D. H., Schechter, A. N., Eastlake, A., and Anfinsen C. B. (1972) *Proc. Natl. Acad. Sci. U.S.A. 69*, 3790−3794.
13. Stanfield, R. L., Fieser, T. M., Lerner, R. A., and Wilson, I. A. (1990) *Science 248*, 712−719.
14. Muller, S., Plaue, S., Samama, J. P., Valette, M., Briand, J. P., and Van Regenmortel, M. H. V. (1990) *Vaccine 8*, 308−314.
15. Spangler, B. D. (1991) *J. Immunol. 146*, 1591−1595.
16. Arnon, R., Maron, E., Sela, M., and Anfinsen, C. B. (1971) *Proc. Natl. Acad. Sci. U.S.A. 68*, 1450−1455.
17. Satterthwait, A. C., Arrhenius, T., Hagopian, R. A., Zavala, F., Nussenzweig, V., and Lerner, R. A. (1989) *Philos. Trans. R. Soc. London B 323*, 565−572.
18. Kaumaya, P. T., VanBuskirk, A. M., Goldberg, E., and Pierce, S. K. (1992) *J. Biol. Chem. 267*, 6338−6345.
19. Cabezas, E., and Satterthwait, A. C. (1999) *J. Am. Chem. Soc. 121*, 3862−3875.
20. Baker, E. N., and Hubbard, R. E. (1984) *Prog. Biophys. Mol. Biol. 44*, 97−179.
21. Stanfield, R. L., Cabezas, E., Satterthwait, A. C., Stura, E. A., Profy, A. T., and Wilson, I. A. (1999) *Structure 7*, 131−142.
22. LaRosa, G. J., Davide, J. P., Weinhold, K., Waterbury, J. A., Profy, A. T., Lewis, J. A., Langlois, A. J., Dreesman, G. R., Boswell, R. N., Shadduck, P., Holley, L. H., Karplus, M., Bolognesi, D. P., Matthews, T. J., Emini, E. A., Putney, S. D. (1990) *Science 249*, 932−935.
23. Nardalli, B., Lu, Y. A., Shiu, D. R., Delpierre-Defoort, C., Profy, A. T., and Tam, J. P. (1992) *J. Immunol. 148*, 914−920.
24. Ahlers, J. D., Pendleton, C. D., Dunlop, N., Minassian, A., Nara, P. L., and Berzofsky, J. A. (1993) *J. Immunol. 150*, 5647−5665.
25. Tolman, R. L., Bednarek, M. A., Johnson, B. A., Leanza, W. J., Marburg, S., Underwood, D. J., Emini, E. A., and Conley, A. J. (1993) *Int. J. Pept. Protein Res. 41*, 455−466.
26. Long, R. D., and Moeller, K. D. (1997) *J. Am. Chem. Soc. 119*, 12394−12395.
27. Vu, H. M., Myers, D., de Lorimier, R., Matthews, T. J., Moody, M. A., Heinly, C., Torres, J. V., Haynes, B. F., and Spicer, L. (1999) *J. Virol. 73*, 746−750.
28. Barbas III, C. F., Collet, T. A., Amberg, W., Roben, P., Binley, J. M., Hoekstra, D., Cababa, D., Jones, T. M., Williamson, R. A., Pilkington, G. R., Haigwoods, N. L., Cabezas, E., Satterthwait, A. C., Sanz, I., and Burton, D. R. (1993) *J. Mol. Biol. 230*, 812−823.
29. Gorny, M. K., Xu, J. Y., Karwowska, S., Buchbinder, A., and Zolla-Pazner, S. (1993) *J. Immunol. 150*, 635−643.
30. White-Scharf, M. E., Potts, B. J., Smith, L. M., Sokolowski, K. A., Rusche, J. R., and Silver, S. (1993) *Virol. 192*, 197−206.
31. King, D. S., Fields, C. G., and Fields, G. B. (1990) *Int. J. Pept. Protein Res. 36*, 255−266.
32. Carpino, L. A., Cohen, B. J., Stephens, Jr., K. E., Sadat-Aalaee, S. Y., Tien, J. H., and Langridge, D. C. (1986) *J. Org. Chem. Soc. 51*, 3732−3734.
33. Tam, J. P., Wu, C.-R., Liu, W., and Zhang, J.-W. (1991) *J. Am. Chem. Soc. 113*, 6657−6662.
34. Ellman, G. L. (1959) *Arch. Biochem. Biophys. 82*, 70−77.
35. Tam, J. P. (1988) *Proc. Natl. Acad. Sci. U.S.A. 85*, 5409−5413.

36. Men, Y., Gander, B., Merkle, H. P., and Corradin, G. (1996) *Vaccine 14*, 1442−1450.
37. Wu, J. X., and Satterthwait, A. C., unpublished.
38. Parren, P. W. H. I., Wang, M., Trkola, A., Binley, J. M., Purtscher, M., Katinger, H., Moore, J. P. and Burton, D. R. (1998) *J. Virol. 72*, 10270−10274.
39. VanCott, T. C., Bethke, F. R., Polonis, V. R., Gorny, M. K., Zolla-Pazner, S., Redfield, R. R., and Birx, D. L. (1994) *J. Immunol. 153*, 449−459.
40. Jellis, C. L., Cradick, T. J., Rennert, P., Salinas, P., Boyd, J., Amirault, T., and Gray, G. S. (1993) *Gene 137*, 63−68.
41. Moore, J. P., McCutchan, F. E., Poon, S. W., Mascola, J., Liu, J., Cao, Y., and Ho, D. D. (1994) *J. Virol. 68*, 8350−8364.
42. Seligman, S. J., Binley, J. M., Gorny, M. K., Burton, D. R., Zolla-Pazner, S., and Sokolowski, K. A. (1996) *Mol. Immunol. 33*, 737−745.
43. Rini, J. M., Stanfield, R. L., Stura, E. A., Salinas, P. A., Profy, A. T., and Wilson, I. A. (1993) *Proc. Natl. Acad. Sci. U.S.A. 90*, 6325−6329.
44. Ghiara, J. B., Stura, E. A., Stanfield, R. L., Profy, A. T., and Wilson, I. A. (1994) *Science 264*, 82−85.
45. Ghiara, J. B., Ferguson, D. C., Satterthwait, A. C., Dyson, H. J., and Wilson, I. A. (1997) *J. Mol. Biol. 266*, 31−39.
46. Tugarinov, V., Zvi, A., Levy, R., and Anglister, J. (1999) *Nat. Struct. Biol. 6 (4)*, 331−335.
47. Sibanda, B. L., Blundell, T. L., and Thornton, J. M. (1989) *J. Mol. Biol. 206*, 759−777.
48. Rose, G. D., Gierasch, L. M., and Smith, J. A. (1986) *Adv. Prot. Chem. 37*, 1−109.
49. Prasad, B. V. V., and Balaram, P. (1984) *CRC Crit. Rev. Biochem. 16 (4)*, 307−348.
50. Pease, L. G., Niu, C. H., and Zimmerman, G. (1979) *J. Am. Chem. Soc. 101*, 184−191.
51. Richardson, J. S., and Richardson, D. C. (1989) in *Prediction of Protein Structure and the Principles of Protein Conformation* (Fasman, G. D., Ed.) pp 1−98, Plenum Press, New York.
52. Sarma, A. V. S., Raju, T. V., Kunwar, A. C. (1997) *J. Biochem. Biophys. Methods 34*, 83−98.
53. Wüthrich, K., Billeter, M., and Braun, W. (1984) *J. Mol. Biol. 180*, 715−740.
54. Wüthrich, K. (1986) *NMR of Proteins and Nucleic Acids*, John Wiley, New York.
55. Dyson, H. J., and Wright, P. E. (1991) *Annu. Rev. Biophys. Biophys. Chem. 20*, 519−538.
56. Chandrasekhar, K., Profy, A. T., and Dyson, H. J. (1991) *Biochemistry 30*, 9187−9194.
57. Dyson, H. J., Rance, M., Houghten, R. A., Lerner, R. A., and Wright, P. E. (1988) *J. Mol. Biol. 201*, 161−200.
58. Wüthrich, K. (1986) *NMR of Proteins and Nucleic Acids*, pp 162−166, John Wiley, New York.
59. Wilmot, C. M., and Thornton, J. M. (1988) *J. Mol. Biol. 203*, 221−232.
60. Richardson, J. S. (1981) *Adv. Protein Chem. 34*, 167−339.
61. Wilmot, C. M., and Thornton, J. M. (1990) *Protein Eng. 3*, 479−493.
62. Basus, V. J. (1989) *Methods Enzymol. 177*, 132−149.
63. Defoort, J. P., Nardelli, B., Huang, W., and Tam, J. P. (1992) *Int. J. Pept. Protein Res. 40*, 214−221.
64. Panina-Bordignon, P., Tan, A., Termijtelen, A., Demotz, S., Corradin, G., and Lanzavecchia, A. (1989) *Eur. J. Immunol. 19*, 2237−2242.
65. DiGeorge, A. M., Wang, B., Kobs-Conrad, S. F., and Kaumaya, P. T. P. (1994) in *Peptides: Chemistry, Structure and Biology. Proceedings of the 13th American Peptide Symposium* (Hodges, R., and Smith, J. A., Eds.) pp 732−733, ESCOM Leiden, The Netherlands.
66. Jennings, V. M. (1995) *ILAR J. 37*, 119−125.
67. Hanly, W. C., Artwhol, J. E., and Bennett, B. T. (1995) *ILAR J. 37*, 93−118.
68. Layne, S. P., Merges, M. J., Spouge, J. L., Dembo, M., Nara, P. L. (1991) *J. Virol. 65*, 3293−3300.
69. D'Souza, M. P., Livnat, D., Bradac, J. A., Bridges, S. H. (1997) *J. Infect. Dis. 175*, 1056−1062.
70. Chesebro, B., Wehrly, K., Nishio, J., and Perryman, S. (1996) *J. Virol. 70*, 9055−9059.
71. Bou-Habib, D. C., Roderiquez, G., Oravecz, T., Berman, P. W., Lusso, P., and Norcross, M. A. (1994) *J. Virol. 68*, 6006−6013.
72. Teicher, E., Maron, E., and Arnon, R. (1973) *Immunochemistry 10*, 265−271.
73. Lerner, R. A. (1984) *Adv. Immunol. 36*, 1−44.
74. Calvo, J. C., Perkins, M., and Satterthwait, A. C. (1994) *Peptides: Chemistry, Structure and Biology; Proceedings of the Thirteenth American Peptide Symposium* (Hodges, R., Smith J. A., Eds.) pp 725−726, ESCOM, Leiden, The Netherlands.
75. Calvo, J. C., Chocontá, K. C., Diaz, D., Orozco, O., Espejo, F., Guzman, F., Patarroyo, M. E. (1998) *Peptides: Frontiers of Peptide Science; Proceedings of the 15th American Peptide Symposium* (Tam, J. P., and Kaumaya, P. T. P., Eds.) pp 819−820, Kluwer Academic, Dordrecht, The Netherlands.
76. Smith, A. D., Geisler, S. C., Chen, A. A., Resnick, D. A., Roy, B. M., Lewi, P. J., Arnold, E., and Arnold, G. F. (1998) *J. Virol. 72*, 651−659.
77. Huang, X., Barchi, J. J., Lung, F. D., Roller, P. P., Nara, P. L., Muschik, J., and Garrity, R. R. (1997) *Biochemistry 36*, 10846−10856.
78. Jelinek, R., Terry, T. D., Gesell, J. J., Malik, P., Perham, R. N., and Opella, S. J. (1997) *J. Mol. Biol. 266*, 649−655.
79. Parren, P. W., Mondor, I., Naniche, D., Ditzel, H. J., Klasse, P. J., Burton, D. R., and Sattentau, Q. J. (1998) *J. Virol. 72*, 3512−3519.

BI0003691